Dislocation-Based Finite Element Modelling of Elasto-plastic Material Deformation

A thesis submitted in partial satisfaction

of the requirements for the degree

Master of Science in Mechanical Engineering

by

James Jau-Kai Chiu

2004

The thesis of James Jau-Kai Chiu is approved.

———————————————————————————————————

J. S. Chen

———————————————————————————————————

Gregory Carman

———————————————————————————————————

Nasr M. Ghoniem, Committee Chair

University of California, Los Angeles

2004

To my dear wife Joanne and my family for your everlasting support.

TABLE OF CONTENTS

List of Figures

LIST OF TABLES

Acknowledgments

I want to thank Professor Ghoniem for his generous support and guidance, and Dr. Sharafat and all members of the Computational Nano and Micromechanics Lab for helping me and answering all my questions.

Abstract of the Thesis

Dislocation-Based Finite Element Modelling of Elasto-plastic Material Deformation

by

James Jau-Kai Chiu

Master of Science in Mechanical Engineering

University of California, Los Angeles, 2004

Professor Nasr M. Ghoniem, Chair

The main objective of this work is to develop a physically-based constitutive model for plastic deformation within the framework of Finite Element Elasto-plastic analysis. The Ghoniem-Matthews-Amodel dislocation-based creep model[47] is extended to obtain local stress-strain relationships in the plastic regime. The extended model is then applied to the martensitic steels, HT-9 and F82H at various temperatures simulating constant strain rate tests to obtain local stress-strain relations, specifically the true stress-strain curves. Finite Element Analysis is then performed based on the developed constitutive stress-strain relationships, and the engineering stress-strain curves are obtained. Results show that the dislocation-based model can be calibrated against experiments using microstructural parameters. The engineering stress-strain curves obtained from Finite Element Analysis via ANSYS are correlated with a wide range of experimental data, showing the versatility of the model. It is proposed that such microstructure-based, and experimentally-calibrated model can be confidently used in the prediction of structural deformations under conditions not attainable experimentally or of no experimental results available.

CHAPTER 1

Introduction and Thesis Objectives

1.1 An Introduction to Materials Modelling

In the recent decades, due to the advancements in computing and electronic microscope technologies, a new realm of science of Materials Modelling has gained much attention. Materials Modelling is a tool which is a set of computationally programmed mathematical equations that are based on the micro to nano-scale material parameters, such as dislocations and atoms. By inputting the desired operating conditions of the material, such as temperature, stress, or strain rate, material properties of interest such as true stress-strain relations and high temperature creep curves can be readily predicted. This revolutionary concept is however, still at its development stage. It is one of the objectives of this thesis to implement a type of material model and exam its accuracy and applicability. The objective of this chapter is to provide a brief introduction to the realm of Materials Modelling, a brief introduction to one of the branches of Materials Modelling-the Phenomenological-based Materials Modelling, and an introduction to the overall project objectives.

Materials Modelling or Multiscale Modelling from Ghoniem et al[46] can be described as an

> *analytical and computational ... framework to describe the mechanics*
> *of materials on scales ranging from the atomistic, through the mi-*

crostructure or transitional, and up to the continuum...

Multiscale Modelling or MMM can thus be traced back to the development of Quantum Mechanics and Continuum Mechanics to the more recent frameworks of Molecular Dynamics and Dislocation Dynamics. The necessity of modelling materials with scales ranging from atomic to continuum is to be able to analyze the mechanics of structures from nano to continuum scale. The demand to analyze the structure at nano-scale has increased dramatically due to the recent development in nanotechnology. The ability to integrate the analysis from nano to continuum scale also posses high importance because MMM has promised to predict nano-scale material responses for a continuum-scale structure. Figure 1.1 from Ghoniem et al [22] shows the constraints in terms of space and time for multi-scaled modelling theories.
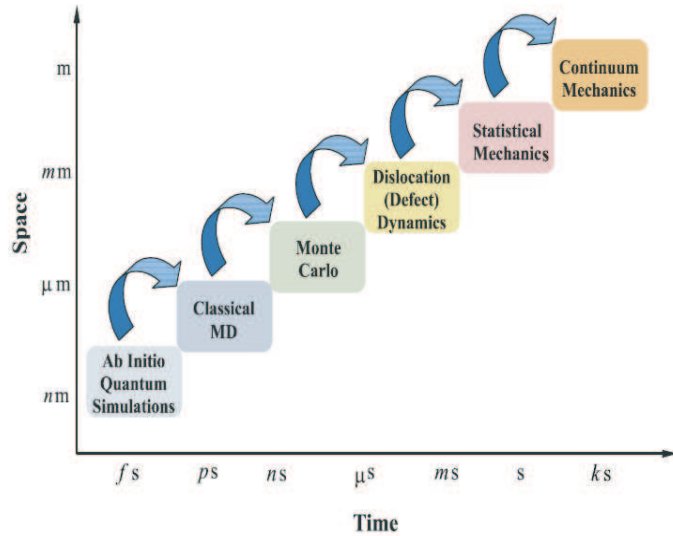
Figure 1.1: Multiscale Modelling Time and Space Constraints

It is the emphasis of MMM to study the plastic deformation of materials from a

mechanics aspect. The importance of plastic deformation from Martinez[35] can be summarized as the following:

- The limitation of experimental data on plastic deformations.

- The size contribution to material strength such as carbon-nanotubes.

- The inhomogeneity of deformation of structures.

One of the Materials Modelling Theory-The Phenomenological or Physical-based Materials Modelling, is a theory that is on the Statistical Mechanics/Continuum Mechanics scale. It is one of the objectives of this thesis to develop a Physical-based Constitutive Model at this scale to study the plastic deformation of certain metal alloys. The following section introduces the Physical-based Plastic Deformation Modelling Theory.

1.2   Significance of the Physical-based Materials Modelling

The Physical-based Materials Modelling for plasticity is based on direct observation of physical phenomenons such as dislocation glide and micro-scaled material parameters such as dislocation densities. Rest of this section will compare this type of plasticity model with other types of plasticity models. There are a number of types of plasticity models that ranged from atomistic to continuum as shown on figure 1.1. The Experimental Model, such as the Johnson-Cook Model[37] is on the continuum scale. The Physical-based Model is different from experimental plasticity models because the Physical-based Models should not have to be parameter-fitted. The following is the experimental Johnson-Cook Model,

$$\sigma = K\varepsilon^n \tag{1.1}$$

where K and n are material parameters to be fitted for different temperatures and materials. The Physical-based Models should be able to deduce local material behaviors if all microstructure parameters have been calibrated correctly.

Another type of MMM theory is Crystal Plasticity. Crystal Plasticity is a Materials Model on the Statistical Mechanics Scale. Developed by Asaro and Rice at 1977, this type of Materials Model treats each grain as a single crystal. The Material deformations are formulated at the grain level for various slip systems. The Macroscopic properties are obtained from averaging the behaviors from all slip systems. The following Busso-McClintock Model[37] is a Crystal Plasticity Model,

$$\dot{F}^p = \{_a\dot{\gamma}_a m^a \otimes n^a\}F^p \tag{1.2}$$

$$\tau_l^a = |\tau^a| - s^a\frac{\mu(T)}{\mu_0} \tag{1.3}$$

$$\dot{\gamma}^a = \dot{\gamma}_0 exp\{-\frac{F_0}{kT}\langle 1 - \langle\frac{\tau_l^a}{\tau_0\mu/\mu_0}\rangle^p\rangle^q\}sgn(\tau^a) \tag{1.4}$$

where a is an individual slip system. The Physical-based Model is different from Crystal Plasticity because the solid is considered as homogeneous for Physical-based Model. Crystal Plasticity considers the solid as non-homogeneous.

Other MMM theories include Dislocation Dynamics, Molecular Dynamics, and Quantum Mechanics which range from the Statistical Mechanics all the way to the atomistic scales. Dislocation Dynamics, pioneered by Ghoniem et al[21] has gained tremendous attention within the past decade. The Physical-based Modelling is different from many of the atomistic models because it requires much less computing resources and the materials are treated homogeneously.

The following summarizes the advantages and disadvantages of applying the Physical-based Models.

Advantages:

- The Model captures the actual physical phenomenons.

- The Model can be solved relatively easy.

- It requires much less computing time.

Disadvantages:

- It is not as localized as the atomistic models.

- Certain physical assumptions still have to be made.

- Certain experimental calibrations are still required.

Even though the current research direction in the realm of Materials Modelling is focused on Dislocation Dynamics, the long computing time of such method still prevents it from being broadly used. The advantages of the Physical-based Models of short computing time and its physical nature, makes it a competitive tool of choice within the range of Multiscale Modelling Theories. The objectives of this thesis will be outlined next.

1.3   Thesis Objectives

The overall objectives of this thesis can be stated as the following:

- Extension and modification of a previously developed model by Ghoniem et al for time-dependent creep deformation to the case of elasto-plastic deformations.

- Calibration of the extended model with the widest possible range of experiments on two ferritic-martensitic steels. The calibration encompasses a considerable range of temperatures and stresses.

- Correlation of the local stress-strain relationships (i.e., constitutive equation) to globally measured engineering stress-strain relationships via Finite Element Modelling.

- Determination of the causes leading to plastic necking and instability in the uniaxial tested specimen.

HT-9 and F82H are the two ferritic-martensitic alloys chosen to be studied. There have been tremendous interests generated by nuclear scientists and engineers in the past three decades in understanding the mechanical and microstructural behavior of certain low activation ferritic-martensitic alloys such as HT-9 and F82H. These alloys can potentially be used to construct the core of fusion reactors due to some of their unique physical properties.

The advantages that these ferritic-martensitic alloys posses include low nuclear activation level after disposed, ability to withstand irradiation induced void swelling, good compatibility with liquid metal coolants, and costs [58]. A wide range of topics on these ferritic-martensitic alloys have been studied. Some of these topics include tensile properties, irradiation induced hardening, ductile to brittle transition temperature, and creep. Both experimental and analytical works have been done within these realms in order to gain better understanding of these alloys.

In recent decades, much emphasis has been placed on understanding the microstructure of materials and its relationship with the material macroscopic properties. One of the most important microstructure parameters of metal alloys is dislocation.

Dislocations are material line defects that have been found to have strong correlation with the yield strength and the inelastic deformation of metal alloys. Much work have been done in recent decades to understand dislocations and its interactions within the materials. The foundations of dislocation theories have

been pioneered by Read[64], Cottrell[11], Friedel[18], and Hirth[36] in the second half of the twentieth century.

In the recent decade, dislocation theories have been formulated into various Physical-based Models that could predict material properties at various conditions. The dislocation-based creep model by Ghoniem, Matthews, and Amodeo[47] was one of the models. Developed to study and predict creep behavior for ferritic-martensitic alloys mentioned earlier, this model has proven to be successful. It is now one of the objectives of this present thesis to extend the Ghoniem-Matthrews-Amodeo Creep Model into a Constitutive Model to study the stress-strain behaviors of these alloys in the plastic regime.

A number of Physical-based Models based on dislocation theories will be presented in the following chapter. Chapter 3 will outline and discuss the formulations of the dislocation based Physical Model developed by Ghoniem et al. Chapter 5 lists and discusses the findings from executing the developed Constitutive Model, and Chapter 6 discusses the conclusions derived from executing the model and examining the results.

CHAPTER 2

Previous Research

In this chapter, a number of dislocation density based materials models will be reviewed and compared. Again, the reasons for formulating materials models based on dislocations is to accurately capture the physical behaviors of materials at a micro-scale as the previous chapter had mentioned. The applications of such models can be used in either creep or constitutive predictions as one would see in this chapter.

The development of physical or dislocation based materials models can be traced back to the 1950's. Some of the earliest scientists and metallurgists were working to explain the work-hardening or softening behaviors of various FCC or BCC metals, specifically on the stage II hardening of FCC metal crystals. It was generally concluded by many through experimental studies and theoretical formulations that a flow stress model for a metal crystal can be formulated by a unique relationship correlating the flow stress and the square root of the dislocation density, and an evolutionary equation of the dislocation density. However, there were no consensus on how exactly the stress-dislocation equation should be formed, and how to describe the complex dislocation evolutionary phenomenon.

Some of the earliest works to formulate the dislocation evolutionary phenomenon include those by Seeger et al[4] on dislocation pile-ups, and Basinski[6] on forest dislocations. Some of the earliest comprehensive models were formed by Kocks[38], Bergström et al[7][61], and later by Mecking and Kocks[31] which

was the milestone K-M Model. The first comprehensive model, the Bergström model[7] will be discussed first.

2.1   The Bergström Model

The Bergström model was intended to predict homogeneous deformation, the deformation from the onset of plastic deformation until the onset of necking for BCC α-Fe at room temperature. One can begin to summarize the model by the following,

$$\sigma = \sigma_i + \sigma^* + \sigma_d \tag{2.1}$$

where σ_i is the athermal strain independent stress, σ^* is the strain rate and dislocation dependent thermal stress, and σ_d is the long-range interaction dependent term. σ^* and σ_d are expressed as the following,

$$\sigma^* = \sigma_u |\frac{\dot{\varepsilon}}{\Phi b L}|^{1/m^*} \tag{2.2}$$

$$\sigma_d = \alpha G b \sqrt{\rho} \tag{2.3}$$

where $\dot{\varepsilon} = \Phi b L v$. Φ is an orientation factor(0.5 for polycrystalline), b is the Burgers vector, L is the density of mobile dislocations, and v is the average velocity of the mobile dislocations. v can be calculated as $v = |\frac{\sigma^*}{\sigma_u}|^{m*}$, where σ^* is the effective stress acting on a dislocation, σ_u is the effective stress giving the dislocation an average unit velocity, and m^* is the temperature-dependent material constant. From 2.2 and 2.3, 2.1 can be then expressed as

$$\sigma = \sigma_i + \sigma_u |\frac{\dot{\varepsilon}}{\Phi b L}|^{1/m^*} + \alpha G b \sqrt{\rho} \tag{2.4}$$

The evolutionary rate equation for the immobilized dislocations ρ_i can be expressed as the following

$$\frac{d\rho_i}{d\varepsilon} = U - \frac{dr}{d\varepsilon} - \frac{da}{d\varepsilon} \tag{2.5}$$

9

where U is the rate at which the mobile dislocation dislocations is increased by creation and or re-mobilization processes, $\frac{dr}{d\varepsilon}$ is the rate at which immobilized dislocations are re-mobilized, and $\frac{da}{d\varepsilon}$ is the annihilation rate. It has been assumed that the mobile dislocation density is much smaller than the total dislocation density, thus the total dislocation density ρ can be approximately as the immobile dislocation density ρ_i. U can be calculated as inversely proportional to the mean free path of the mobile dislocation as the following.

$$U(t) = \frac{vL}{s(t)} \tag{2.6}$$

The term $\frac{dr}{d\varepsilon}$, the rate at which immobilized dislocations are re-mobilized can be simply written as the following

$$\frac{dr}{d\varepsilon} = \theta_1 \rho_i \tag{2.7}$$

where θ_1 is a material constant independent of strain, and ρ_i is the immobile dislocation density. The annihilation term $da/d\varepsilon$ is divided into three processes by Bergström. They are mobile dislocation annihilating each other, mobile and immobile dislocations annihilate each other, and mobile dislocation annihilating with microstructure surfaces such as grain boundaries. It has been postulated by Bergström that the mobile dislocations annihilation rate is proportional to the square of the mobile dislocation density. The immobile and mobile dislocation annihilation rate is proportional to the product of mobile and immobile dislocation densities, and the mobile to surface annihilation rate is proportional to the product of the strain independent annihilation space L and the mobile dislocation density. $da/d\varepsilon$ can then be expressed as the following

$$\frac{da}{d\varepsilon} = \lambda_1 L^2 + \lambda_s L \rho_i + \theta N L \tag{2.8}$$

where λ_1, λ_2, and θ_2 are strain independent constants. From 2.6, 2.7, and 2.8, 2.5 can be written as the following, assuming that the mobile dislocation is time

independent.

$$\frac{d\rho_i}{d\varepsilon} = U(\varepsilon) - \theta_1\rho_i - \lambda_1 L^2 - \lambda_2 L\rho_i - \theta_2 NL \simeq \frac{d\rho}{d\varepsilon} = U(\varepsilon) - A - \Omega\rho \qquad (2.9)$$

$$A = (\lambda_1 - \lambda_2)L^2 + (\theta_2 N - \theta_1)L \qquad (2.10)$$

$$\Omega = \theta_1 + \lambda_2 L \qquad (2.11)$$

If U, the rate of immobilization and annihilation of mobile dislocations are assumed to be strain independent, and Ω, the probability of re-mobilization and annihilation between immobile and mobile dislocations is assumed to be small, then the following stress strain relation can be attained.

$$\sigma = \sigma_{i0} + \alpha Gb\{\frac{U-A}{\Omega}(1 - e^{-\Omega\varepsilon}) + \rho_0 e^{-\Omega\varepsilon}\}^{1/2} \qquad (2.12)$$

$$\sigma_{i0} = \sigma_i + \sigma_u[\frac{\dot{\varepsilon}}{\Phi bL}]^{1/m^*} \qquad (2.13)$$

The above model has been extended to predict behaviors of FCC polycrystallines from [61]. From [61] 2.6 can be expressed as the following,

$$U(\varepsilon) = \frac{1}{100\theta bs(\varepsilon)} \qquad (2.14)$$

where θ is an orientation factor about 0.5 for BCC and 0.32 for FCC. For FCC, due to fewer slip systems and limited cross slip, the dislocation evolutionary equation can be modified to be the following,

$$\frac{d\rho}{d\varepsilon} = \frac{1}{100\theta b[s_0 + (s_1 - s_0)e^{-k\varepsilon}]} - \Omega\rho \qquad (2.15)$$

where s is the mean free path of mobile dislocation. s_0 is an equilibrium value, and s_1 is the initial condition of s at $\varepsilon = 0$. If $\Omega = 0$, then the stress strain relation can be revised to be the following,

$$\sigma = \sigma_{i0} + \alpha Gb\{\rho_0 + U_0\varepsilon + \frac{U_0}{k}ln(\frac{s_0 + (s_1 - s_0)e^{-k\varepsilon}}{s_1})\}^{1/2} \qquad (2.16)$$

11

where $\rho_0 = \rho$ at $\varepsilon = 0$ and $U_0 = 1/100\theta bs_0 = 1/bs_0$. [7] and [61] are limited to uniaxial strain with homogeneous deformation under ambient temperatures. Modified model by Bergström et al have taken higher temperature deformations into consideration[65]. It was proposed by Bergström from experimental studies that the recovery parameter Ω should be separated into an athermal and a thermal term as the following.

$$\Omega = \Omega_0 + \Omega(\dot{\varepsilon}, T) \tag{2.17}$$

From some of the well studied assumptions regarding recovery that the thermal term of recovery is due to vacancy and interstitial diffusions of dislocations with subgrain walls. Incorporating the assumptions in [65], the thermal recovery term can be written as the following,

$$\Omega(\dot{\varepsilon}, T) = \{kn_0(2D_0)^{1/2}\}^{2/3}exp(-\frac{Q_m}{3RT})\dot{\varepsilon}^{-1/3} \tag{2.18}$$

where k and D_0 are constants. n_0 is the number of vacancies per unit volume, and Q_m is the vacancy migration energy. The validity of the above model has been shown in [7], [61], and [65] to correlate quite well with experimental results. Despite its well organized dislocation evolutionary equation(3 parameters, U, A, and Ω), its treatment on the contribution of various types of dislocations (mobile, immobile) would be further advanced by other models[47].

2.2 Kocks-Mecking Model

Kocks and Mecking[31] formulated a similar model and is now known as the Kocks-Mecking (KM) model. This model will be discussed next. The KM model is similar to the Bergström model because it utilizes the square root of the dislocation density relation with the flow stress. Therefore, the following kinetic

12

equations were proposed,

$$\hat{\sigma} = \hat{\alpha}\mu b\sqrt{\rho} \tag{2.19}$$

$$\sigma = s(\dot{\varepsilon}, T)\hat{\sigma} \tag{2.20}$$

where $\hat{\sigma}$ is a reference flow stress at a reference temperature, and $\hat{\alpha}$ is a constant depending on the dislocation interactions. The flow stress at a finite temperature is described by 2.20 as the product of s and the reference stress $\hat{\sigma}$. If other resistance such as lattice resistance, solution hardening, and grain size effects are taken into consideration, then 2.20 can be extended to be

$$\sigma = \alpha(\dot{\varepsilon}, T)\mu b\sqrt{\rho} + \sigma_0(\dot{\varepsilon}T) \tag{2.21}$$

The evolutionary equation is expressed as the rate between the dislocation storage and dynamic recovery as the following,

$$\frac{d\rho}{d\varepsilon} = \frac{1}{\Lambda b} - L_r N_r \frac{v_r}{\dot{\varepsilon}} \tag{2.22}$$

where Λ is the mean free path. L_r is the dislocation length. N_r is the number of dislocation per unit volume, and v_r is the rate of recovery. The reference stress $\hat{\sigma}$ and the flow stress σ is correlated by the following,

$$s(\dot{\varepsilon}, T) \equiv \frac{\sigma}{\hat{\sigma}} = (\frac{\dot{\varepsilon}}{\dot{\varepsilon}_0})^{1/m} \tag{2.23}$$

where m is a temperature dependent constant. It has been pointed out by Kocks and Mecking that 2.23 is not sufficient to describe dynamic recovery and the "transient" behavior. Therefore, 2.23 can be modified as the following to accommodate dynamic recovery,

$$s = (\frac{\dot{\varepsilon}}{\dot{\varepsilon}_0})^{1/m} exp(-F\frac{\theta_r}{\theta_h}) \tag{2.24}$$

$$s = (\frac{\dot{\varepsilon}}{\dot{\varepsilon}_0})^{1/m}(1 - F\frac{\theta_r}{\theta_h}) \tag{2.25}$$

where θ_h is the athermal hardening rate and θ_r is the recovery rate. This one parameter model has been found to work quite well under continuous deformation such as constant strain rate or stress[15], and its formulation is simple and elegant. The work of Estrin et al[15], [16], [66] has extended the KM model to predict material deformation for more complicated loading scenarios, which will be discussed next.

2.3 The Estrin Model

From the work by Estrin et al[15], 2.22 can be re-written as

$$d\rho/d\varepsilon = k_1\rho^{1/2} - k_2\rho \tag{2.26}$$

where k_1 and k_2 are constants. From 2.19 and 2.26, that the following evolution equation can be written,

$$d\hat{\sigma}/d\varepsilon = \theta_0(1 - \hat{\sigma}/\hat{\sigma}_s) \tag{2.27}$$

where

$$\theta_0 = \alpha G b k_1/2 \tag{2.28}$$

$$\hat{\sigma}_s = \alpha G b(k_1/k_2) \tag{2.29}$$

From [15], the kinetic equation that relates the flow stress and the hardness parameter $\hat{\sigma}$ can be shown to be

$$\sigma/\hat{\sigma} = (\dot{\varepsilon}/\hat{\dot{\varepsilon}})^{1/m} \tag{2.30}$$

where m is a temperature dependent constant. Equations 2.27, 2.28, 2.29, and 2.30 constitutes the Estrin Model, which is very similar to the KM Model. Estrin et al have proposed a modified version of the above model[66] [16], and it will be

14

presented in the following paragraphs. One can begin the modified Estrin Model
with the Lévy-von Mises equation

$$\dot{\varepsilon_{ij}}^p = \frac{3}{2}\frac{\dot{\varepsilon}^p}{\sigma}s_{ij} \tag{2.31}$$

$$\dot{\varepsilon_{ij}} = \dot{\varepsilon_{ij}}^e + \dot{\varepsilon_{ij}}^p \tag{2.32}$$

where

$$\dot{\varepsilon}^p = \sqrt{\frac{2}{3}\dot{\varepsilon_{ij}}^p\dot{\varepsilon_{ij}}^p} = \dot{\varepsilon_0}(\frac{\sigma}{\hat{\sigma}})^m \tag{2.33}$$

$$\sigma = \sqrt{\frac{3}{2}s_{ij}s_{ij}} = \hat{\sigma}(\frac{\dot{\varepsilon}^p}{\dot{\varepsilon_0}})^{1/m} \tag{2.34}$$

The structure parameter $\hat{\sigma}$ can be expressed as the function of dislocation density
ρ as the following,

$$\hat{\sigma} = M\alpha Gb\sqrt{\rho} \tag{2.35}$$

where M is the average Taylor factor. The evolution equation is the following,

$$d\rho/d\varepsilon^p = k_1\sqrt{\rho} - k_2\rho \tag{2.36}$$

where the constant k_1 is associated with dislocation storage, and the constant
k_2 is associated with dislocation annihilation by recovery. The strain rate and
temperature dependent constant k_2 can be obtained by the following,

$$k_2 = k_{20}(\frac{\dot{\varepsilon}^p}{\dot{\varepsilon_0^*}})^{-1/m} \tag{2.37}$$

where k_{20} is a constant. n and $\dot{\varepsilon_0}^*$ are temperature dependent constants. If
constant plastic strain rate is assumed, then equations 2.33 to 2.37 can be solved.
The following is the stress-strain relation,

$$\frac{\sigma - \sigma_s}{\sigma_i - \sigma_s} = exp(-\frac{\varepsilon^p - \varepsilon_i^p}{\varepsilon_{tr}}) \tag{2.38}$$

15

where

$$\sigma_s = M\alpha Gb\frac{k_1}{k_{20}}(\frac{\dot{\varepsilon^p}}{\dot{\varepsilon_0}})^{1/m}(\frac{\dot{\varepsilon^p}}{\dot{\varepsilon_0^*}})^{1/n} \tag{2.39}$$

$$\varepsilon_{tr} = \sigma_s/\Theta_{II} \tag{2.40}$$

$$\Theta_{II} = \frac{1}{2}M^2\alpha Gbk_1(\frac{\dot{\varepsilon^p}}{\dot{\varepsilon_0^*}})^{1/m} \tag{2.41}$$

If forming process such as hot forming, which the phenomenon of static recovery due to dislocation climb must be included, 2.36 can be modified as the following,

$$d\rho/d\varepsilon^p = k_1\sqrt{\rho} - k_2\rho - r/\dot{\varepsilon^p} \tag{2.42}$$

where

$$r = r_0 exp(-\frac{U_0}{k_B T})\sinh\frac{\beta\sqrt{\rho}}{k_B T} \tag{2.43}$$

r_0 is a constant, U_0 is the activation energy, β is constant, and k_B is the Boltzmann constant. The above model has been shown by Estrin et al to match experimental results quite well. However, if simulating non-monotonic deformation is necessary, then the "one-parameter" model such as the Estrin and the KM model would not be sufficient. The following model[66] proposed by Estrin et al tackles the case of cyclic deformation. The "two-parameter" model by Estrin et al for a monotonic loading case begins with the following kinetic equation between the inelastic strain ε^{in} and the applied stress σ.

$$\dot{\varepsilon}^{in} = \xi\{\frac{|\sigma|}{\sigma_0\sqrt{Y}}\}^m X sign(\sigma) \tag{2.44}$$

X and Y are internal variables and defined as

$$X(t) = \frac{\rho_m(t)}{\rho_m(0)} \tag{2.45}$$

$$Y(t) = \frac{\rho_f(t)}{\rho_f(0)} \tag{2.46}$$

where ρ_m is the mobile dislocation density and ρ_f is the immobile or forest dislocation density at time t. The evolutionary equations for the internal variables

16

X and Y with respect to the inelastic strain are defined as the following,

$$\frac{\partial X}{\partial |\varepsilon^{in}|} = [-C - C_1\sqrt{Y} - C_3X + C_4\frac{Y}{X}]q \qquad (2.47)$$

$$\frac{\partial Y}{\partial |\varepsilon^{in}|} = C + C_1\sqrt{Y} - C_2Y + C_3X \qquad (2.48)$$

where q is $\rho_f(0)/\rho_m(0)$. The coefficients C to C_4 all bear physical significance such as C, which models the effect of nonshearable second-phase particles or grain boundaries. For details, see [66]. For a cyclic loading case, an additional internal variable Z must be introduced to account for recoverable dislocations that trapped at the subgrain walls, ρ_{ri}. The additional evolutionary equations due to Z is the following.

$$\frac{\partial Z}{\partial t} = (C_5\sqrt{Y} - C_2Z)\dot{\varepsilon}^p - C_6Z \qquad (2.49)$$

where $Z = \rho_{ri}(t)/\rho_{ri}(0)$. The evolutionary equation for X, equation 2.47 would have to be modified to be

$$\frac{\partial X}{\partial t} = (-C - C_1\sqrt{Y} - C_3 + C_4\frac{Y}{X} + C_7^*Z)q|\dot{\varepsilon}^{in}| \qquad (2.50)$$

where $C_7^* = C_7$ for $|\sigma| < \sigma_0\sqrt{Y}$, 0 otherwise. The kinetic equation 2.44 must be modified and an additional back stress σ_{back} must also be introduced as the following.

$$\frac{\partial \sigma_{back}}{\partial \varepsilon^{in}} = C_8\sqrt{Y}sign(\dot{\varepsilon})^{in} - C_9\sigma_{back} \qquad (2.51)$$

$$\dot{\varepsilon}^{in} = \xi\{\frac{|\sigma| - |\sigma_{back}|}{\sigma_0\sqrt{Y}}\}^m sign(\sigma - \sigma_{back}) \qquad (2.52)$$

The above cyclic loading model has been found to match experimental results quite well. For experimental details, see [66]. Gottstein et al[27][20] have proposed other multi-parameter dislocation based models. The Gottstein models will be outlined in the following section.

2.4 The Gottstein Model

The Gottstein Model was proposed by Gottstein et al[27] at 1987 to study and predict metallurgical behaviors under creep(constant stress) and constant strain rate testings. The derivation of the model begins with the following assumption of dislocations.

$$d\rho = d\rho^+ + \sum_i d\rho_i^- \qquad (2.53)$$

$d\rho^+$ is the dislocation production and $d\rho_i^-$ denotes the contribution of various recovery mechanisms. The strain increment is represented as

$$d\varepsilon = d\varepsilon_{DIS} + d\varepsilon_{SUB} \qquad (2.54)$$

where $d\varepsilon_{DIS}$ is glide of mobile dislocation and $d\varepsilon_{SUB}$ is the collective subgrain dislocation movements. The production rate $d\rho^+$ can be represented as

$$d\rho^+ = d\varepsilon_{DIS}/bL \qquad (2.55)$$

where L the slip length is inversely proportional to the mean free path as $L = \kappa/\sqrt{\rho}$. The subgrain movement $d\varepsilon_{SUB}$ is the following,

$$d\varepsilon_{SUB} = \rho_{SUB} b v_{SUB} \frac{d\varepsilon}{\dot{\varepsilon}} \qquad (2.56)$$

where ρ_{SUB} is the subgrain dislocation density. From 2.54 to 2.56, the production rate with subgrain movement can be obtained as.

$$d\rho^+ = d\varepsilon \left(\frac{\sqrt{\rho}}{b\kappa} - \frac{1}{\dot{\varepsilon}\kappa} \rho_{SUB} v_{SUB} \sqrt{\rho} \right) \qquad (2.57)$$

Provided that $\rho_{SUB} = \beta\rho$, the average subgrain size $d = \frac{\lambda}{\sqrt{\rho}}$, the subgrain velocity $v_{SUB} = m\lambda\beta b\gamma\sigma$, and the recovery process as the following,

$$\rho^- = d\rho_{GLIDE}^- + d\rho_{CLIMB}^- + d\rho_{SUB}^- \qquad (2.58)$$

where

$$d\rho_{GLIDE}^{-} = -\frac{L_R}{b}\rho d\varepsilon \tag{2.59}$$

$$d\rho_{CLIMB}^{-} = -\frac{D_c}{\chi}\rho^2 dt = -\frac{D_c}{\chi}\rho^2\frac{d\varepsilon}{\dot{\varepsilon}} \tag{2.60}$$

$$d\rho_{SUB}^{-} = -\frac{\rho_{SUB}v_{SUB}}{d}\frac{d\varepsilon}{\dot{\varepsilon}} \tag{2.61}$$

L_R is the swept-up line length per recovery site, and D_c is the diffusion constant for the climb process. The evolutionary equation according to can then be expressed as the following,

$$d\rho = d\varepsilon\{\frac{\sqrt{\rho}}{b\kappa} - \frac{L_R}{b}\rho - (\frac{D_c}{\chi} + M\sigma[1 + \frac{\lambda}{\kappa}])\frac{\rho^2}{\dot{\varepsilon}}\} \tag{2.62}$$

where $M = m\beta^2 b$. For the case of constant strain rate test, the flow stress is related to dislocation density by the common equation.

$$\tau = \alpha\mu b\sqrt{\rho} \tag{2.63}$$

From 2.62 and 2.63, the hardening coefficient θ can be obtained as.

$$\theta \equiv \frac{d\tau}{d\varepsilon} = \frac{\alpha\mu}{2\kappa} - \frac{L_R}{2b}\tau - (\frac{D_c}{\chi} + M\sigma[1 + \frac{\lambda}{\kappa}])\frac{\tau^3}{2(\alpha\mu b)}\frac{1}{\dot{\varepsilon}} \tag{2.64}$$

For the case of a creep test, the following strain rate expression can be derived.

$$\dot{\varepsilon} = \frac{\Phi}{\sqrt{\rho}} + M\lambda b\sigma\rho^{3/2} = \frac{1}{\sqrt{\rho}}(\Phi + M\lambda b\sigma\rho^2) \tag{2.65}$$

The steady state stress, transient creep, steady state creep can then be studied by the above model. The three-parameter model was further modified by Gottstain et al[20] to account for more physical phenomenons such as precipitate hardening and to account for multiple slip systems by introducing the Taylor factor. The external stress can be found by the following relation,

$$\sigma_{ext} = M(f_i\tau_i + f_w\tau_w) \tag{2.66}$$

19

where M is the Taylor factor. f_i, τ_i and f_w, τ_w are volume fractions and resolved shear stress of subgrain(cell) interior and wall. The effective shear stress is related to the dislocation density as the following.

$$\tau_x = \tau_{eff_x} + \alpha G b \sqrt{\rho_x}, \quad x = i, w \qquad (2.67)$$

The following kinetic equation, the Orowan equation, is used to solve for the effective shear stress under constant strain rate,

$$\dot{\gamma} = \dot{\varepsilon} M = \rho_m b v \qquad (2.68)$$

where $\dot{\gamma}$ is the shear strain rate, and v is the glide velocity as given by the following.

$$v = \lambda v_0 exp(-\frac{Q}{k_B T}) \sinh(\frac{\tau_{eff} V}{k_B T}) \qquad (2.69)$$

λ is the jump width-the mean spacing of obstacles, v_0 is the attack frequency, Q is the effective activation energy for glide, and V is the activation volume. The evolutionary equations for the three parameters can be summarized as the following,

$$\dot{\rho_m} = \dot{\rho_m}^+ - \dot{\rho_m}^{-,lock} - \dot{\rho_m}^{-,anni} - \dot{\rho_m}^{-,dip} = \frac{\dot{\varepsilon} M}{b L_{eff}} -$$

$$4 d_{lock} \frac{\dot{\varepsilon} M}{b} \frac{n-1}{n} \rho_m - 2 d_{anni-c} \frac{\dot{\varepsilon} M}{b} \frac{1}{n} \rho_m - 2(d_{dip} - d_{anni-c}) \frac{\dot{\varepsilon} M}{b} \frac{1}{n} \rho_m \qquad (2.70)$$

$$\dot{\rho_i} = \dot{\rho_i}^+ - \dot{\rho_i}^- = \dot{\rho_m}^{-,lock} - 2 d_{anni-g} v_{climb} \frac{1}{n} \rho_i^2 \qquad (2.71)$$

$$\dot{\rho_w} = \dot{\rho_w}^+ = \frac{1}{f_w} \dot{\rho_m}^{-,dip} \qquad (2.72)$$

Please see [20] for details of the parameters in the above equations. The model summarized above has been shown to be able to predict the mechanical material behavior quite well for two-phase aluminium alloys at elevated temperatures, and has been interfaced with Finite Element Analysis for crystal plasticity. There are many other models that are based on subgrain structures and multi-parameters. The following section will briefly highlight these other models.

2.5 Other Models

Some of the other models and microstructure formulations include ones by Lagneborg et al[51], which is based on formulating a dislocation distribution frequency function $\Phi(l)$. The evolutionary equations are then formulated by integrating the frequency function. The model by Prinz et al[19] was formulated based upon a plastic resistance τ to glide. Once the plastic resistance is solved, the plastic strain can then be solved. Blum et al[63][62][44][52], further investigated the non-monotonic loading conditions for creep, and has deduced a number of models, specifically basing on the composite model developed by Mughrabi et al[42][43], to explain various mechanisms such as glide and recovery. Similar works have also been done by Argon et al[5] and Zehetbauer[68] on FCC Metals. The works by Nabarro[45] on diffusional creep and the works by Gittus[26][23] on dislocation creep have also laid great foundations for the recent works in the area of dislocation based materials modelling.

CHAPTER 3

Model Development

The dislocation based constitutive model is based on the dislocation creep model developed by Ghoniem et al[47]. The dislocation based creep model was initially developed to predict high temperature deformation under arbitrary time-dependent stress and temperature histories for engineering materials in harsh environments. One of the applications of the creep model is to predict creep for ferritic alloys such as HT-9 and F82H. These alloys have been considered as the materials for the core of nuclear fusion reactors due to their low activation nature and good ability to withstand irradiation induced void swelling. HT-9 and F82H will also be the materials investigated by this dislocation based constitutive model as previously stated.

The dislocation creep model is a comprehensive model based on a compilation of developments in creep theory from recent decades such as the work by Nabarro[45] and Gittus[26] which were previously mentioned, and such as the works by Bullough et al[50] on rate theory. The objective of developing this dislocation based constitutive model is to be able to apply this model to Finite Element Analysis, and to study mechanical material behaviors for the alloys mentioned above. The studying of the ability to model the Mechanical behaviors of strain softening is also another subject of interest. Works by Heald et al[28] and Bullough et al[8] on irradiation creep mentioned in [47] are also possible directions of future investigations via this model. The inclusion of subgrain microstructure evolution is a

key aspect of this model. The processes of subgrain evolution has been reviewed by Holt[29] as mentioned by Ghoniem et al[47]. The details of the development of the dislocation based constitutive model will be explained in the following. This dislocation based constitutive model is composed of six rate equations to predict the behavior of six engineering parameters, namely the creep strain, the mobile, static and boundary dislocation density, the subgrain radius, and the applied stress.

3.1   Model Assumptions

A number of references(Takeuchi et al[56], Langdon[39], Challenger et al[9], Michel et al[13], and Cuddy[12]) on the investigations of subgrain and high temperature alloy characteristics were summarized by Ghoniem et al [47]. This paper will briefly re-summarize these characteristics and assumptions as a point of departure to develop the dislocation based constitutive model. The following can be stated about alloys operating at high temperatures.

- Dislocation pileups and debris due to cold works are not observed

- Dislocation form a polygonal network called subgrains, and they nucleate at high enough temperatures

- The applied stress is inversely proportional to the dimension of the subgrains

- The dislocation density within the subgrains are low, and increases with the square of the applied stress

- The formation of subgrains may be delayed to higher temperatures in materials with lower stacking fault energy

- Subgrain growth may be inhibited by solute-hardened alloys

- Subgrains are commonly seen in materials with low stacking fault energy, extensive precipitation, and substantial concentration of hardening solutes

The various dislocation processes discussed by Gittus[23], Li[40], and Sandström[54][53] can be summarized as the following.

- Multiplications of dislocations within the subgrains

- Annihilation of mobile dislocations within the subgrains

- Annihilation of dislocations at the subgrain walls

- Absorbtion of dislocations by the subgrain walls

- Emissions of dislocations by the subgrain walls

- Nucleation of new subgrains

- Growth of subgrains by coalescence

These phenomenons described above were modelled by Ghoniem et al[47] to study dislocation creep. It is the objective of this paper to study constant strain rate (CSR) test based on the original model.

3.2 Dislocation multiplication and immobilization

The model is commenced by the Orowan equation as the following, which is used as the kinetic equation for this dislocation based constitutive model.

$$d\varepsilon^p/dt = b\rho_m v_g \tag{3.1}$$

ε^p is the creep or plastic strain. ρ_m is the mobile dislocation density, which is the dislocation density within the moving dislocation density within the subgrain. v_g is the glide velocity, and b is the Burger's vector. The glide process is assumed to be easy, and the effect the climb is ignored. Since this is a uniaxial model, only one slip system is considered. Therefore the value of b, the burger's vector can be obtained from empirical references. However, the instantaneous value of the mobile dislocation density and glide velocity would have to be formulated.

It is understood that the subgrains provide a source and also act as barriers for mobile dislocations. In order to form a rate equation for dislocation, the rate of dislocation production and annihilation must be formulated. From [47], the rate of the mobile dislocation is produced within the subgrains is formulated as the frequency of the dislocation produced multiplied by the number of dislocation produced. It can shown as the following.

$$\dot{\rho_m} = \rho_m^{3/2} v_g \tag{3.2}$$

The frequency of production is $\rho_m^{1/2} v_g$, where $\rho_m^{1/2}$ is the reciprocal of the mean free path of the mobile dislocations. The effects of subgrain wall and subgrain radius would also have to be considered. The potential density of source can be characterized as $\frac{1}{2}h^2 R_{sb}$, where h is the dislocation spacing within the subgrains, and R_{sb} is the subgrain radius. The dislocation spacing within the wall, h can be formulated as the following, where ρ_s and ρ_b are static and boundary dislocations.

$$h = 1/(\rho_s + \rho_b)R_{sb} \tag{3.3}$$

From the above, two rate equations can be formulated as the following.

$$\dot{\rho_m} = \beta \rho_s R_{sb} v_g / h^2 - \rho_m v_g / 2R_{sb} \tag{3.4}$$

$$\dot{\rho_s} = \rho_m v_g / 2R_{sb} \tag{3.5}$$

where β is a density factor. It is apparent that the immobilization term of equation 3.4 is equation 3.5.

3.3 Internal stress

The internal stress must be analyzed since the effective stress, which is a function of internal stress, will be incorporated in the formulation of dislocation velocity. Again, from [47], the internal stress is caused by any opposition to dislocation motions, and this opposition can be characterized into three sources. The first source is any precipitates and other dislocations that oppose dislocation motions. The internal stress that mobile dislocations must overcome is $\mu b / 2\pi\lambda$, where λ is the effective obstacle spacing, and μ is the shear modulus. In the case where both precipitate and dislocation obstacles are present, the effective obstacle spacing λ is given as the following.

$$\lambda = 1/(1/\lambda_d + 1/\lambda_p) \tag{3.6}$$

λ_d is the inter-dislocation spacing, and is given as $\lambda_d = 1/\rho_m^{1/2}$. λ_p is the inter-precipitate spacing, and is given as $\lambda_p = 1/(N_p r_p)^{1/2}$, where N_p is the volume concentration of precipitates, and r_p is the mean radius.

The second source of opposition are the dislocations that have not yet neutralized their long range stress fields. Essentially these dislocations have not moved into their low energy configuration. The mobile dislocations could be accelerated or retarded depending on the nature of these un-neutralized stress fields. These unstable dislocations are static dislocations within the subgrains. The boundary dislocations themselves do not contribute to the internal stress beyond a distance greater than the average dislocation distance within the subgrains[18]. Combining the effects of precipitates and unstable static dislocations. The long range internal

stress can be expressed as the following.

$$\sigma_i = \mu b / 2\pi\lambda + \zeta\mu b\rho_s^{1/2} \tag{3.7}$$

The third source of opposition is the friction resistance to glide from over-sized solutes. These typically are solute particles used to strengthen metals. From [47], for well-annealed materials without hardening precipitates and heat treatment, this stress can be identified as the initial flow stress, σ_0. Therefore, the effective stress, σ_e can be represented as the following, where σ_a is the applied stress.

$$\sigma_e = \sigma_a - \sigma_i - \sigma_0 \tag{3.8}$$

3.4   Dislocation velocity

From[47], the dislocation velocity does not contribute significantly to the steady state creep strain rate. However, the dislocation velocity does affect the transient creep strain rate, and its relationship with stress, dislocation density affects the long term strain rate as well. The formulation of dislocation velocity can primarily be dictated by the effect of solute atoms. The following formulation given by[57][10], accounts for the viscous nature of dislocation movement under low stress

$$v_g = D_a kTb\sigma_e / [c_0(\beta^*)ln(R/r)] \tag{3.9}$$

where σ_e is the effective stress, c_0 is the uniform volume concentration of the solute, D_a is the solute diffusion coefficient, R is the outer cutoff radius, and r is the inner cutoff radius. The value of β^* is given by [36]

$$\beta^* = (\mu b / 3\pi)[(1 + \nu)/(1 - \nu)](v_s - v_a) \tag{3.10}$$

where ν is the Poisson's ration, v_s is the solute atomic volume, and v_a is the matrix atomic volume. When solute atoms are trapped at the core of the dislocations,

the following equation can be formulated[36]

$$v_g \approx 2bv_d exp(-2_a/kT)sinh(\sigma_e b^2 l_a/kT) \tag{3.11}$$

where v_d is the dislocation vibrational frequency, W_a is the activation free energy for core diffusion of the solute, and l_a is the spacing of the solute atoms in the core. Another empirical formulation for the dislocation velocity is the following.

$$v_g = a_1 exp(-W_g/kT)\sigma_e\Omega/kT \tag{3.12}$$

where a_1 and W_g are parameters to be fitted, and Ω is the atomic volume. If the effect of cutting of the obstacle is considered, the following can be formulated.

$$v_g = v_d\lambda sinh(\sigma_e b^2 \lambda/2kT)exp(-U_g/kT) \tag{3.13}$$

U_g is the activation energy for the process, which is approximately twice the jog formation energy.

3.5 Climb and Recovery

The phenomenon of dislocation climb contributes to the recovery of dislocations over time. The effect of climb recovery is considered to be the climb of dislocation dipoles into the subgrains. The effective stress the dislocation dipoles exert on each other can be expressed as the following, where s is the separation distance between the dipoles.

$$\sigma_c = \mu b/2\pi(1-\nu)s \tag{3.14}$$

The vacancy concentration near the dislocations c_{vd}^c will be enhanced or reduced depending on the vacancy interaction. If the thermal equilibrium concentration is c_v^c, then c_{vd}^c can be expressed as the following.

$$c_{vd}^c = c^c exp(\pm\frac{\sigma_c\Omega}{kT}) \simeq c^c(1 \pm \frac{\sigma_c\Omega}{kT}) \tag{3.15}$$

28

The net flow of vacancies into dislocations can be expresses as the following rate equation under irradiation.

$$\frac{dq_d}{dt} = k_{id}^2 D_i c_i - k_{vd}^2 D_v c_v + k_{vd}^2 D_v c_{vd} \tag{3.16}$$

k_{id}^2, D_i, and c_i are the dislocation sink strength for interstitial, interstitial diffusion coefficient, and the interstitial bulk concentration. k_{vd}^2, D_v, and c_v are equivalent parameters for vacancies. The interstitial and vacancy concentration can be expressed by the following rate equations

$$\frac{\partial c_i}{\partial t} = K + k_i^2 D_i c_i - \alpha c_i c_v \tag{3.17}$$

$$\frac{\partial c_v}{\partial t} = K + k_v^2 D_v c_v - \alpha c_i c_v \tag{3.18}$$

where K is the rate of production of Frenkel pais, k_i^2 and k_v^2 are the sum of the sink strength from all the potential sinks for interstitial and vacancies, Kv^e is the sum of the vacancy emission rates for all the sinks, α is the rate constant for interstitial and vacancies. The sink strength, according to Rauh and Bulllogh[49], can be expressed as

$$k_{\alpha N}^2 = -\frac{\pi \rho_N}{ln[(1/2)e^\gamma (k_\alpha L_\alpha)]} \simeq -\frac{2\pi \rho N}{ln(k_\alpha L_\alpha)} \tag{3.19}$$

where the subscript α refers to either interstitial or vacancy, N refers to network dislocations, and γ is Euler's constant, ~ 0.5772. L_a is a length parameter that governs the range of interactions between dislocations and defects.

$$L_\alpha = (1 + \nu)\mu b |\triangle V_\alpha|/3\pi(1 - \nu)kT \tag{3.20}$$

$\triangle V_\alpha$ is the relaxation volume of the defect, and it is typically -0.5Ω for vacancy and 1.2Ω for interstitial. The difference between vacancies and interstitial has been considered as the cause for irradiation induced swelling. If the dislocation network is the only sink for vacancies, then 3.19 can be approximated as

$$k_{\alpha N}^2 = -2\pi \rho_N/ln(\rho_N^{1/2} L_\alpha) \tag{3.21}$$

The transfer of defects into jobs on the dislocation is controlled by the following

$$\eta_\alpha = c_j b(a_{\alpha c} v_{\alpha c}) exp(-\triangle W_\alpha/kT) \tag{3.22}$$

where c_j is the job concentration, $a_{\alpha c}$ and a_α are the geometric factors, $v_{\alpha c}$ and v_c are the attempt frequency for jumps, and $\triangle W_\alpha$ is the difference in activation energy. Argon and Moffatt[2] have proposed a revised 3.22 to be the following

$$\eta_\alpha = 10^3 f_\alpha c_j b(\Gamma/\mu b)^2 \tag{3.23}$$

where γ is the stacking fault energy. Taking transfer rate into consideration, 3.19 becomes the following.

$$k_{\alpha d}^2 = 2\pi\eta_\alpha\rho_N/[1 - \eta_\alpha ln(\rho_N^{1/2} L_\alpha)] \tag{3.24}$$

Since dislocation dipoles are the primary interest, the sink strength for dipoles according to Hirth[36] becomes

$$k_{\alpha d}^2 = 2\pi\eta_\alpha\rho_N/[1 - \eta_\alpha ln(k_\alpha^2 L_\alpha s)] \tag{3.25}$$

where s is the dipole separation distance. Assuming no irradiation effect, then 3.16 reduces to

$$\frac{dq_d}{dt} = k_{vd}^2 D_s\sigma_c\Omega/kT \tag{3.26}$$

where the lattice self-diffusion coefficient $D_s = D_v c_v^e$. The climb velocity is

$$v_c = (dq_d/dt)/b\rho_d \tag{3.27}$$

From 3.14, 3.25, 3.26, and 3.27, the dipole separation can be expressed as

$$ds/dt = -2\eta D_s\mu\Omega/(1-\nu)skT[1 - \eta ln(k_\alpha^2 L_\alpha s)] \tag{3.28}$$

3.28 can be integrated with initial dipole separation s_0 to be the following.

$$\tau = -\frac{(1-\nu)kT}{4D_s\mu\Omega}s_0^2[\eta_v ln(k_v^2 L_v s) - \frac{\eta_v}{2} - 1] \simeq \frac{s_0}{4v_c} \tag{3.29}$$

The mobile dislocation recovery rate can be expressed as the following, assuming all dislocations are part of the recovery process, and the initial dipole separation is $s_0 = \rho_m^{-1/2}$.

$$\dot{\rho}_m = -\frac{2\rho_m}{\tau} = -8\rho_m^{3/2}v_{cm} \tag{3.30}$$

The static dislocation recovery can be expressed as the following, assuming that the initial dipole separation is $s_0 = h$ and $k_v^2 = 1/h^2$.

$$\dot{\rho}_s = -\frac{2\rho_s}{\tau} = -8\rho_s\frac{v_{cs}}{h} \tag{3.31}$$

A possibility of diffusion short-circuited by the dislocation core has been investigated by Evans et al[17]. The flux of vacancies along the dislocation can be expressed as.

$$j_p = 2\eta_v D_p \sigma_e \Omega / (b + \eta_v L_p)kT \tag{3.32}$$

where η_v is the transfer coefficient of vacancies from dislocation to jobs. D_p is the core diffusion coefficient, and L_p is the path length for diffusion along core. If jog spacing is much less than the diffusion path length, the 3.32 can be reduced to

$$j_p = 2D_p\sigma e\Omega / L_p kT \tag{3.33}$$

The climb velocity is then

$$v_c = 2\pi b D_p \sigma_c \Omega / L_p^2 kT \tag{3.34}$$

3.6   Dynamic Recovery

The dynamic recovery phenomenon is one of the most important phenomenons for the model. Dynamic recovery explains the saturation of strain hardening because it supposes that the mobile dislocations of opposite signs would annihilate each

other over time. This phenomenon is first recognized by Johnson and Gilman[34], and Webster[60], and can be expressed as the following,

$$\dot{\rho_m} = -\delta(\dot{\rho_m} + \rho_s)\dot{\varepsilon}/b = -\delta\rho_m(\rho_m + \rho_s)v_g \tag{3.35}$$

where δ is a length parameter between dislocations characterizing annihilations[50][14]. 3.35 explains the saturation of strain hardening[59].

3.7 Stability of subgrains

The grain boundary evolution can be modelled as the product of driving pressure and mobility[47]. The grain boundary energy per unit area, γ_{sb} for low-angle subgrain boundary can be expressed as

$$\gamma_{sb} = -\frac{\mu b^2}{4\pi(1-\nu)}\rho_b R_{sb} ln(bR_{sb}\rho_b) \simeq \frac{\mu b^2}{3}\rho_b R_{sb} \tag{3.36}$$

The total energy of one subgrain E, is $4\pi R_{sb}^2 \gamma sb$. The subgrain grows by boundary coalescing of collapsing small subgrains. The total force acting on a boundary for a collapsing subgrain can be expressed as.

$$\frac{dE}{dR_{sb}} = \frac{\partial E}{\partial R_{sb}} + \frac{\partial E}{\partial \rho_b}\frac{d\rho_b}{dR_{sb}} \tag{3.37}$$

The pressure for subgrain growth is.

$$P_{sb} = (1/4\pi R_{sb}^2)(dE/dR_{sb}) = (4/3)\mu b^2 \rho_b \tag{3.38}$$

It can be assumed that the movement of dislocations are glide and climb within the subgrains. The following form for core mobility can be assumed.

$$M_{sb}^c = 2\pi b D_p \Omega/h^2 kT \tag{3.39}$$

For lattice diffusion

$$M_{sb}^L = 2\pi \eta_v D_v \Omega/h^2 kT \tag{3.40}$$

If the effect of precipitates are introduced, the pressure of growth must satisfy the following[3][54].

$$P_{sb} \geq 2\pi r_p^2 N_p \gamma_{sb} \tag{3.41}$$

If 3.41 is satisfied, then the subgrain evolution can be approximated as

$$\partial R_{sb}/\partial t = M_{sb}(P_{sb} - 2\pi r_p^2 N_p \gamma_{sb}) \tag{3.42}$$

If the subgrain motion is controlled by the motion of precipitates, one example of mobility can be expressed as

$$M_{sb} = D_s \Omega / 4\pi r_p^4 N_p kT \tag{3.43}$$

It can be assumed that the driving force for nucleation can be of the form $\mu b(\rho^{1/2} - K_c/2R_{sb})$, where ρ is the sum of the mobile and static dislocations densities. K_c is a constant with a value around 10[24][25]. The time to nucleate the new subgrain configuration can be expressed as

$$\tau = (kT/\mu \eta_v K_c \rho^{1/2} D_s)[\rho^{1/2} - (Kc/2Rsb)]\Omega \tag{3.44}$$

The dislocations have to move a distance of approximately $K_c \rho^{1/2}$ to reach a new configuration. The cell radius change is $R - (K_c/2\rho^{1/2})$. The above expressions can be combined to obtain the following rate equation for subgrain radius.

$$\partial R_{sb}/\partial t = -\mu \eta_v K_c R_{sb}[(\rho_m + \rho_s)^{1/2} - (K_c/2R_{sb})]^2 \Omega D_s/kT \tag{3.45}$$

3.45 is only applicable when $(\rho_m + \rho_s)^{1/2} > K_c/2R_{sb}$.

3.8   Constitutive Relation

The total uniaxial strain can be decomposed into the elastic and the plastic strain as the following[41].

$$\varepsilon = \varepsilon^e + \varepsilon^p \tag{3.46}$$

From Hooke's Law, it is known that

$$\sigma = E\varepsilon^e \qquad (3.47)$$

where E is the young's modulus. From 3.46 and 3.47, the following rate equation can then be established.

$$\dot{\sigma} = E(\dot{\varepsilon} - \dot{\varepsilon}^p) \qquad (3.48)$$

3.9 Model Summary

The overall model can be summarized as the following.

Creep Strain-Orowan Equation

$$d\varepsilon^p/dt = b\rho_m v_g \qquad (3.49)$$

Mobile Dislocation Density

$$\frac{\partial \rho_m}{\partial t} = v_g[\rho_m^{3/2} + \frac{\beta R_{sb}}{h^2} - \frac{\rho_m}{2R_{sb}} - 8\rho_m^{3/2}(\frac{v_{cm}}{v_g}) - \delta\rho_m(\rho_m + \rho_s)] \qquad (3.50)$$

Static Dislocation Density

$$\frac{\partial \rho_s}{\partial t} = v_g[(\frac{\rho_m}{2R_{sb}}) - 8\frac{\rho_s}{h}(\frac{v_{cs}}{v_g}) - \delta\rho_m\rho_s] \qquad (3.51)$$

Boundary Dislocation Density

$$\frac{d\rho_b}{dt} = 8(1 - 2\zeta)\rho_s\frac{v_c}{h} - (\frac{\rho_b}{R_{sb}})M_{sb}(p_s - 2\pi r_p^2 N_p \gamma_{sb}) \qquad (3.52)$$

Subgrain Radius

$$\frac{dR_{sb}}{dt} = M_{sb}(p_s - 2\pi r_p^2 N_p \gamma_{sb}) - \mu\eta_v K_c R_{sb}[(\rho_m + \rho s)^{1/2} - \frac{K_c}{2R_{sb}}]\frac{\Omega D_s}{kT} \qquad (3.53)$$

The Constitutive Relation has been added to calculate stress as a function of the total strain.

Constitutive Relation

$$\frac{d\sigma}{dt} = E(\frac{d\varepsilon^{tot}}{dt} - b\rho_m v_g) \tag{3.54}$$

CHAPTER 4

Model Implementation

The Ghoniem-Matthews-Amodeo (GMA) Model has been implemented for constant stress (creep) test[1]. This chapter will explain the implementation of the GMA Model for constant strain rate (CR) test. The following outlines the steps taken to implement the model.

1. Model Programming-The model must first be converted into a computer program. Then the Model, now a set of Ordinary Differential Equations, can be solved via numerical methods simultaneously to obtain the true stress-strain curves

2. Model Calibration-Calibrate the computer generated stress-strain curves with published experimental data

3. FEA Implementation-Interface the calibrated true stress-strain curves with Finite Element Software packages, i.e., ANSYS

4. Result Comparison-Compare with the published data to determine the FEA accuracy. This will be discussed in detail in the next chapter

The steps above will be discussed in detail in the following.

4.1 Model Programming

The GMA Model has been implemented by Ghoniem et al[47] to study creep. Therefore, the structure of the programming is very similar to what Ghoniem et al have done. However, the existing implementation has to be modified to study constitutive relations. The following will explain the structure of the programming. The programming language of choice is FORTRAN90. This language has been chosen because of the ease of modification from the existing FORTRAN program written by Amodeo[47]. The program has been divided into three subroutines, the main subroutine, the diffun subroutine, and the DLSODE subroutine. The following describes functions of each subroutine.

4.1.1 The Main Subroutine

The functions of the main subroutine are to:

- provide an User Interface

- house initial conditions

- call DLSODE subroutine to calculate the values of each dependent variables(ρ_m, ρ_s, etc.,)

- write the output to a text file

The algorithm for the main subroutine are shown on figure 4.1. Note that the user is allowed to choose to study either creep or constant strain rate test, and the choice dictates the value of the parameter "NEQ", number of equations to solve. If one chooses to study creep, then NEQ is set to five. If one chooses to study constant strain rate, then NEQ is set to six. The outputs are then adjusted accordingly.
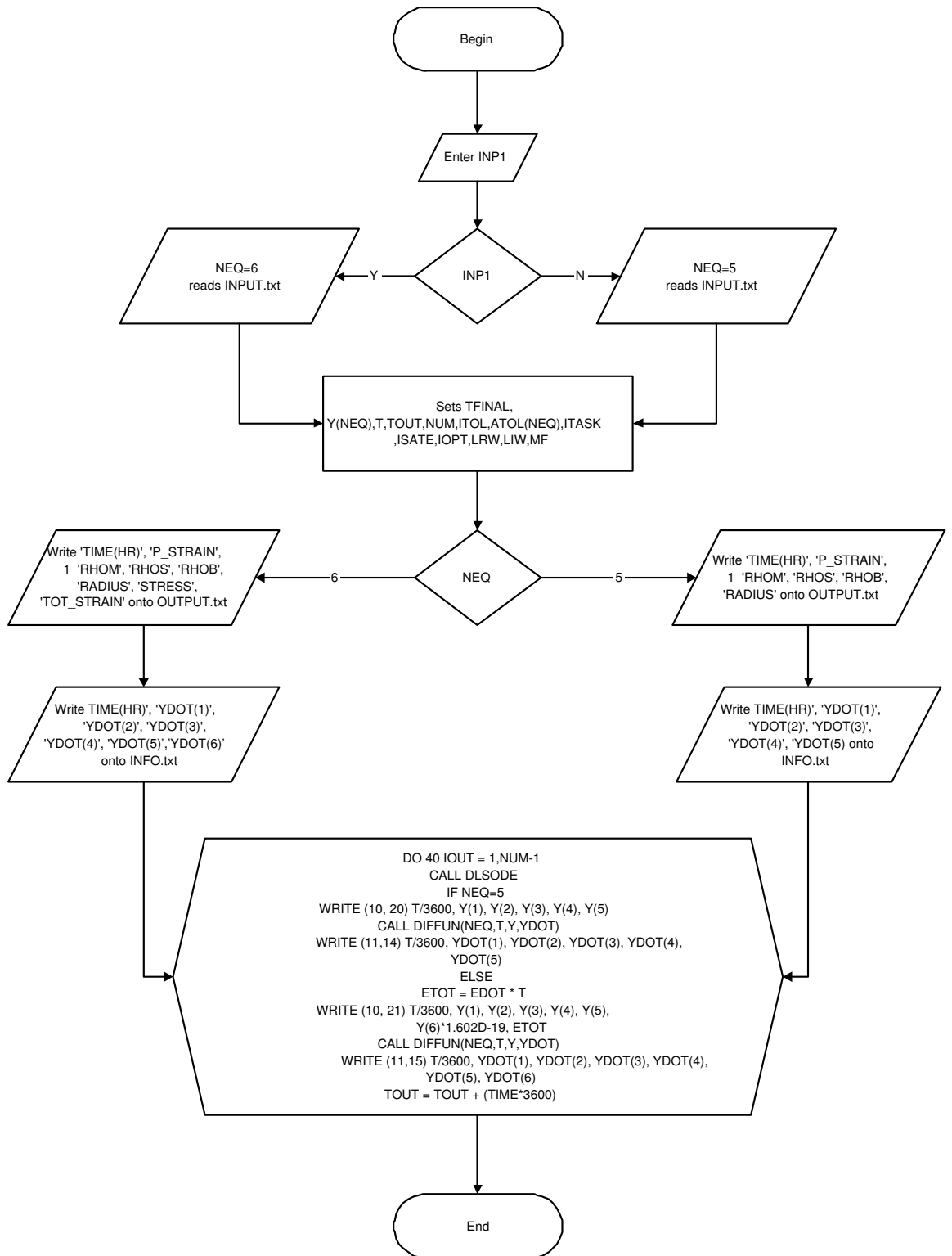
Begin

Enter INP1

INP1

Y → NEQ=6
reads INPUT.txt

N → NEQ=5
reads INPUT.txt

Sets TFINAL,
Y(NEQ),T,TOUT,NUM,ITOL,ATOL(NEQ),ITASK
,ISATE,IOPT,LRW,LIW,MF

NEQ

6 → Write 'TIME(HR)', 'P_STRAIN',
1 'RHOM', 'RHOS', 'RHOB',
'RADIUS', 'STRESS',
'TOT_STRAIN' onto OUTPUT.txt

5 → Write 'TIME(HR)', 'P_STRAIN',
1 'RHOM', 'RHOS', 'RHOB',
'RADIUS' onto OUTPUT.txt

Write TIME(HR)', 'YDOT(1)',
'YDOT(2)', 'YDOT(3)',
'YDOT(4)', 'YDOT(5)','YDOT(6)'
onto INFO.txt

Write TIME(HR)', 'YDOT(1)',
'YDOT(2)', 'YDOT(3)',
'YDOT(4)', 'YDOT(5) onto
INFO.txt

DO 40 IOUT = 1,NUM-1
CALL DLSODE
IF NEQ=5
WRITE (10, 20) T/3600, Y(1), Y(2), Y(3), Y(4), Y(5)
CALL DIFFUN(NEQ,T,Y,YDOT)
WRITE (11,14) T/3600, YDOT(1), YDOT(2), YDOT(3), YDOT(4),
YDOT(5)
ELSE
ETOT = EDOT * T
WRITE (10, 21) T/3600, Y(1), Y(2), Y(3), Y(4), Y(5),
Y(6)*1.602D-19, ETOT
CALL DIFFUN(NEQ,T,Y,YDOT)
WRITE (11,15) T/3600, YDOT(1), YDOT(2), YDOT(3), YDOT(4),
YDOT(5), YDOT(6)
TOUT = TOUT + (TIME*3600)

End

Figure 4.1: Flow Chart Algorithm of Main Subroutine

Table 4.1: HT-9 and F82H Constants

Parameter	Units	Value of HT-9	Value of F82H
Glide energy, E_{glide}	eV	2.5	2.4
Self energy, E_{self}	eV	2.8	2.8
Diffusion coefficient, D_0	cm^2/s	0.2	0.2
Burger's vector, b	cm	2.58E-8	2.58E-8
Atomic volume, Ω	cm^3	1.19E-23	1.19E-23
Precipitate radius, r_p	$\overset{\circ}{A}$	40.5 (at 550 C)	40.5 (at 550 C)
Precipitate concentration, N_p	cm^3	1.63E19 (at 550 C)	1.63E19 (at 550 C)
Jog fraction, X_{jog}	-	0.0455	0.03
Activation volume, Q	Ω	21.5 (at 400 C)	35 (at 400 C)

4.1.2 The Diffun Subroutine

The functions of the diffun subroutine are the following.

- Reads input data

- Lists required constants and computes the necessary functions

- Computes and returns the values of the six ordinary differentials to DL-SODE

Note that the diffun subroutine is called by the DLSODE subroutine to compute the current value of the differentials, YDOT. The common constants for HT-9 and F82H are shown on table 4.1. The information for HT-9 on table 4.1 is from [47], and the information for F82H is approximated from the values of HT-9. The algorithm of the diffun subroutine is shown on figure 4.2.
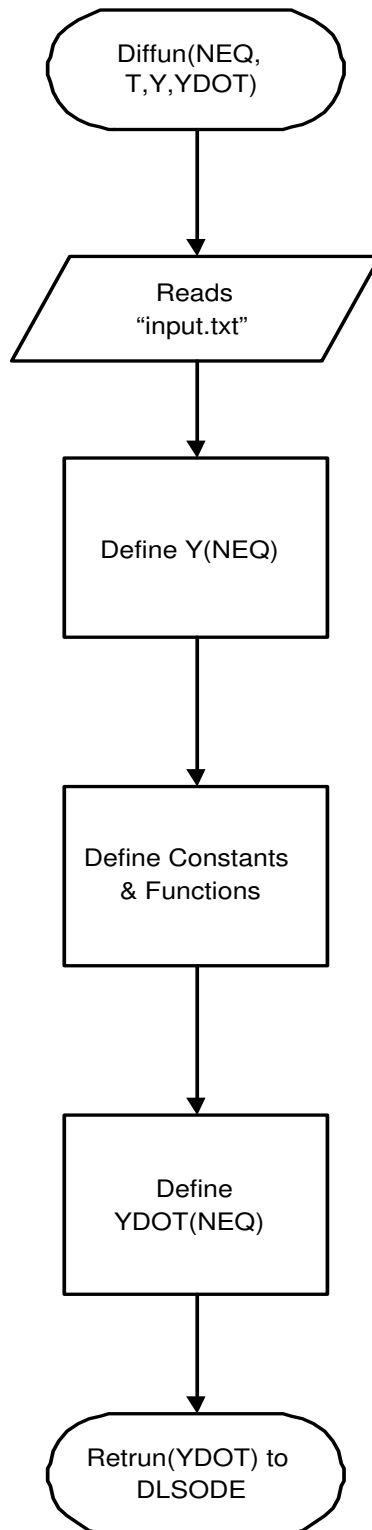
Figure 4.2: Flow Chart Algorithm of Diffun Subroutine

40

Table 4.2: DLSODE Parameter Values	
DLSODE Parameters	Parameter Values
ITOL	2
RTOL	1E-4
ATOL	0
ITASK	1
ISTATE	1
IOPT	0
LRW	437
LIW	30
MF	22

4.1.3 The DLSODE Subroutine

The DLSOLE(Double-precision Livermore Solver for Ordinary Differential Equations) was used as the numeric software code to solve the set of ordinary differential equations. The Livermore Solver(LSODE) provides two versions, the single precision solver (SLSODE) and the double precision solver (DLSODE). The DLSODE version was chosen because it provides higher floating precision. This is necessary because a number of parameters within the model posses values that require double precision allowance. The function of the DLSODE subroutine is to integrate the differentials provided by the Diffun subroutine. Table 4.2 lists the values of the parameters required to be set for the DLSODE subroutine. See [48] for detailed algorithms and descriptions of DLSODE. Once the Model has been programmed, the true stress-strain curves can be obtained. The section below explains this process.

Table 4.3: Input Parameters and Typical Values

Input Parameters	Unit	Typical Values
Time Increment Step, TIME	hours	10/3600
Total Test Time, TFINAL	hours	5/60
Total Strain Rate, EDOT	strain/s	0.0001
Material, METAL	-	HT-9
Test Temperature, TDEGC	C	450

Table 4.4: Output Parameters

Parameter	Unit
Plastic Strain, ε^p	cm/cm
Mobile Dislocation Density, ρ_m	$1/cm^2$
Static Dislocation Density, ρ_s	$1/cm^2$
Boundary Dislocation Density, ρ_b	$1/cm^2$
Subgrain Radius, R_{sb}	cm
Applied Stress, σ	MPa

4.1.4   Model Execution

For a constant strain rate test, a number of input parameters must be set. Table 4.3 lists the required input parameters and the typical values used. For each test execution at a specific temperature, the outputs are written to a text file for each time step increment. One can then plot the total applied stress versus the total strain values to obtain the true stress strain curves for the specific temperature. Figure 4.3 is a sample output for the true stress strain curve, and table 4.4 lists the output parameters.
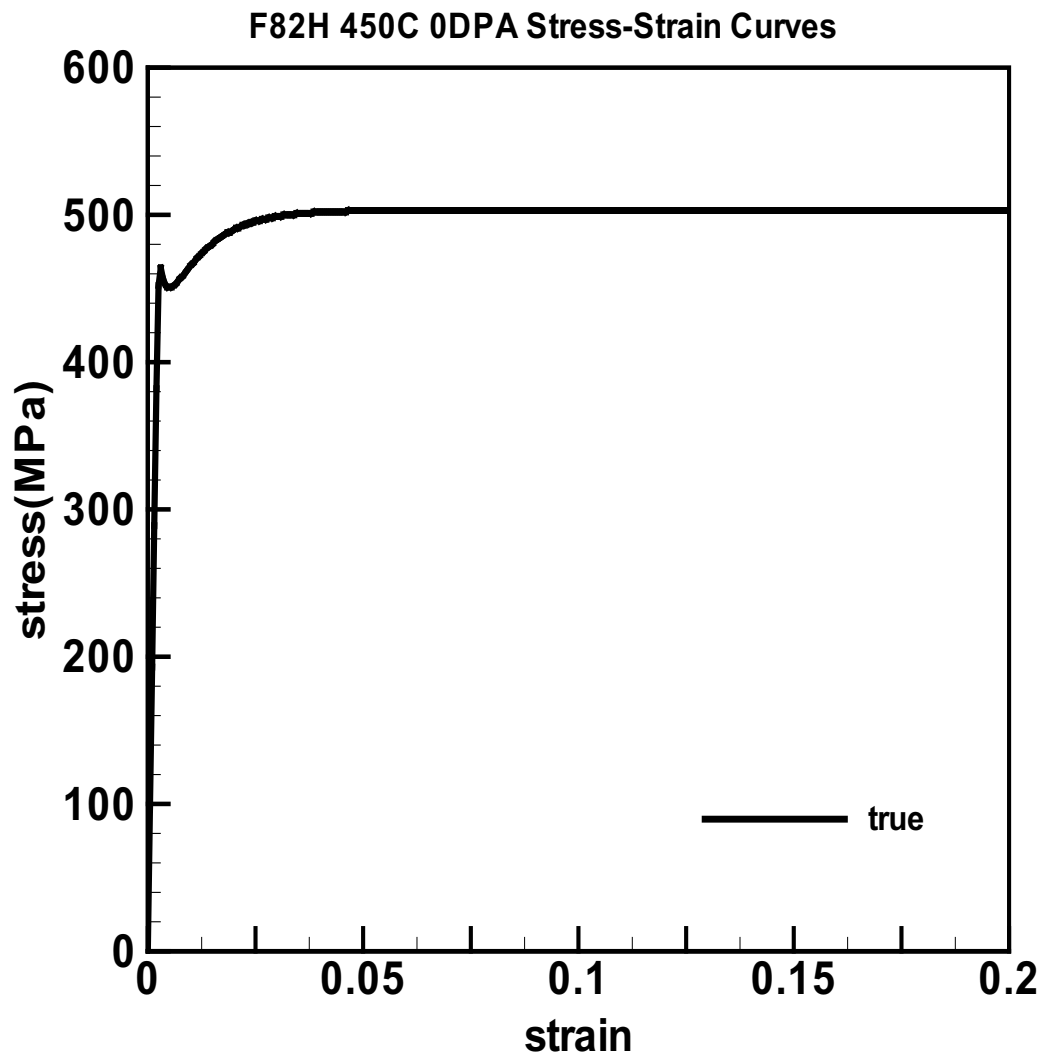
Figure 4.3: True Stress Strain Curve Sample

Table 4.5: Calibration Parameters

Parameter	Unit	Affected Property
Initial Mobile Dislocation Density, $\rho_m(0)$	$1/cm^2$	Yield Strength
Initial Static Dislocation Density, $\rho_s(0)$	$1/cm^2$	Yield Strength
Initial Boundary Dislocation Density, $\rho_b(0)$	$1/cm^2$	Yield Strength
Jog Concentration, X_{jog}	-	Yield Strength
Activation Volume, Q	Ω	Yield Strength
Critical Dislocation Spacing, δ	cm	Elasto-plastic tangent
Precipitate Radius, r_p	Å	Yield Strength
Precipitate Concentration, N_p	cm^3	Yield Strength
Dislocation Vibration Frequency, ν_d	sec^{-1}	Yield Strength

4.2   Model Calibration

When the true stress-strain curve is generated the first time for each temperature, a number of parameters still need to be calibrated so the mechanical properties, such as yield strength and the elasto-plastic tangent would match the experimental results. Table 4.5 and 4.6 lists the calibrating parameters for HT-9 and F82H, and their values and targeted material properties.

The models have been calibrated at 232C, 450C, 550C, and 650C for HT-9 and F82H. The calibration parameter values have been chosen to be within reasonable range of the values published by Ghoniem et al[47]. However, it is true that the validity of the calibration parameter values would have to be further ensured through more rigorous researches.

Table 4.6: Calibration Parameters Values	
Parameter	HT-9/F82H Value
Initial Mobile Dislocation Density, $\rho_m(0)$	1E10/1E8
Initial Static Dislocation Density, $\rho_s(0)$	1E9/1E7
Initial Boundary Dislocation Density, $\rho_b(0)$	1E9/1E7
Jog Concentration, X_{jog}	0.0455/0.03
Activation Volume, Q	21.5/35(at 400C)
Critical Dislocation Spacing, δ	4E-6/6E-6
Precipitate Radius, r_p	40.5/40.5(at 550C)
Precipitate Concentration, N_p	1.63E19/1.63E19 (at 550C)
Dislocation Vibration Frequency, ν_d	1E12/1E12

4.3 Finite Element Implementation

Once the true stress-strain curves can be computed by the model, the curves can then be input as material properties in commercial Finite Element Package to simulate elasto-plastic response. The commercial package ANSYS has been chosen to perform the analysis. The following steps outline the processes to perform elasto-plastic response via ANSYS, and each step will be discussed in the following sections.

1. Model and Mesh Test Specimen

2. Define and Input Material Properties

3. Define Loads

4. Execute Analysis and Obtain Results
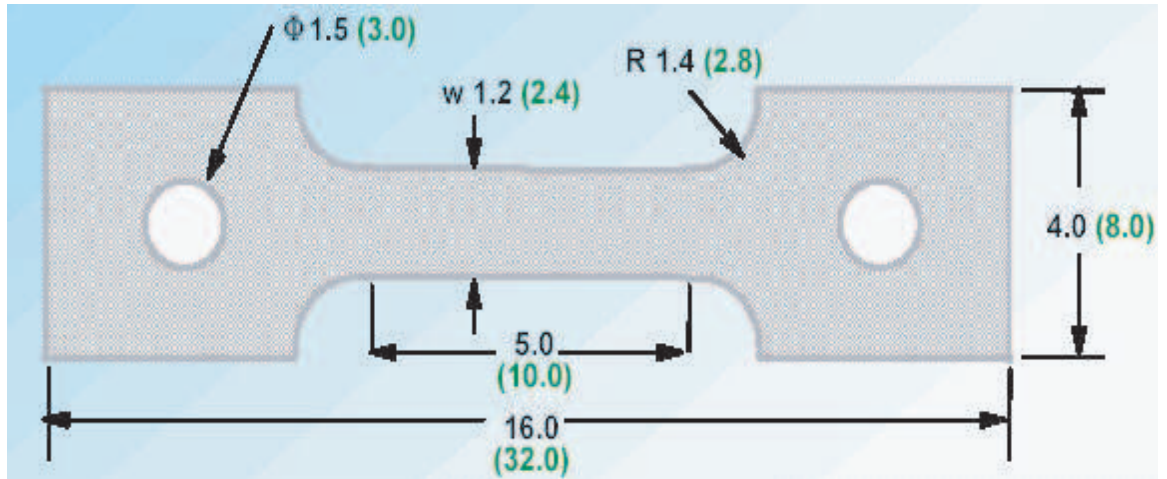
Figure 4.4: Small Test Specimen Dimension

4.3.1 Test Specimen Modelling and Meshing

A small tensile specimen is used as the simulation specimen. The small tensile specimen has been used by many to test mechanical properties of Fusion Alloys after irradiation. The dimension of the specimen is given by [67] as shown on figure 4.4. All dimension units are in millimeters. The specimen has a thickness of 1mm, and a gauge length of 5mm as shown on figure 4.4. Figure 4.5 shows the 3D Model of the specimen. Once the Model has been created, Finite Element Meshes will be applied to the model. Initially 2-dimensional specimen and elements were used. However, convergence instabilities were experienced with 2D plane stress elements. Therefore, an ANSYS 3-dimensional element, SOLID95, was used to mesh the model. SOLID95 is a 3D element with 20 nodes, and each node has 3 degrees of freedom[32] as shown on figure 4.6. The model was divided into three sections for meshing. The Two end sections with ring holes have been meshed by the tetrahedron option of the SOLID95 element due to its ability to adapt to non-rectangular geometry. The middle section has been meshed by the standard

46
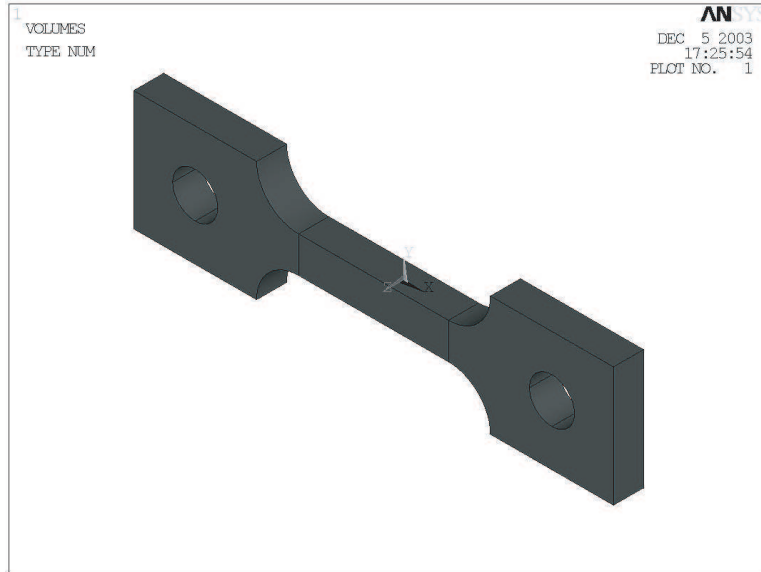
Figure 4.5: Small Test Specimen 3D Model

cube option of the SOLID95 element. Figure 4.7 shows the meshed model. The meshing at the middle section of the specimen has been further refined to allow for more accurate approximation. Once the model has been meshed, the material property must be defined.

4.3.2 Material Property Definition

Table 4.7 lists the material property that must be defined and their typical values. A typical stress strain curve input would be figure 4.3. The type of plastic response would also have to be defined in ANSYS, as this step tells ANSYS what type of algorithm to use to compute the elasto-plastic tangent and the stress. A rate-independent, isotropic hardening plastic response was chosen for the simulation for simplicity. See [33] for algorithm details. The next step would be to define the loads and the boundary conditions to simulate a constant strain rate tensile testing.

47
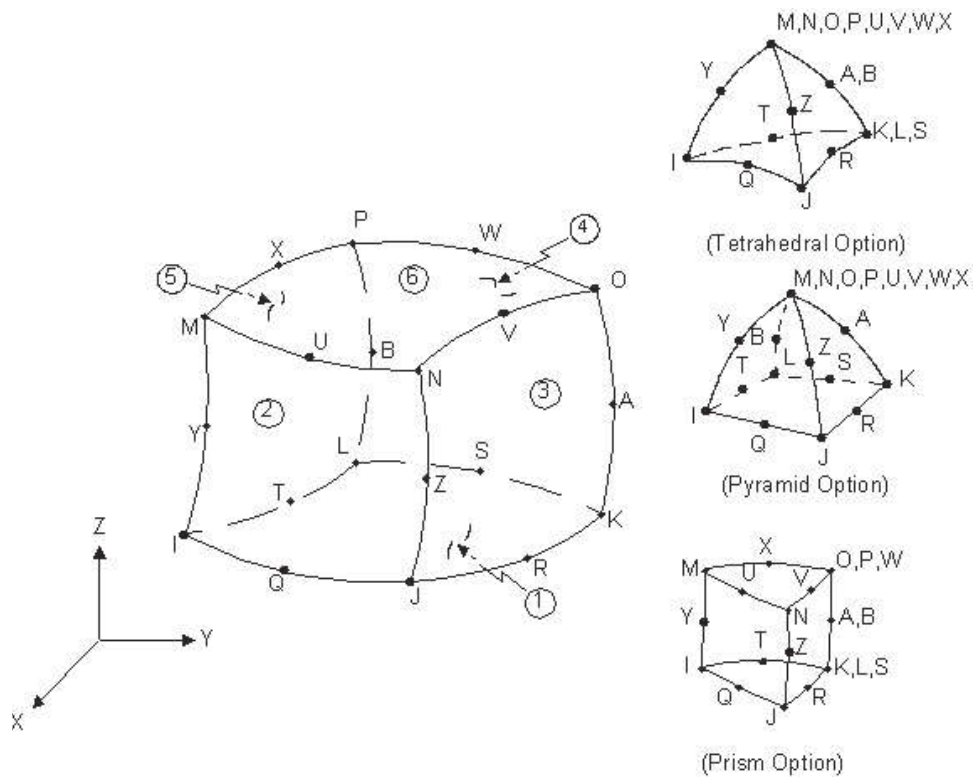
Figure 4.6: SOLID95 Element

Table 4.7: ANSYS Input Material Properties

Material Property	Typical Value
Young's Modulus, E	200(GPa)
Poisson's Ratio, ν	0.29
Stress-Strain Curves	-
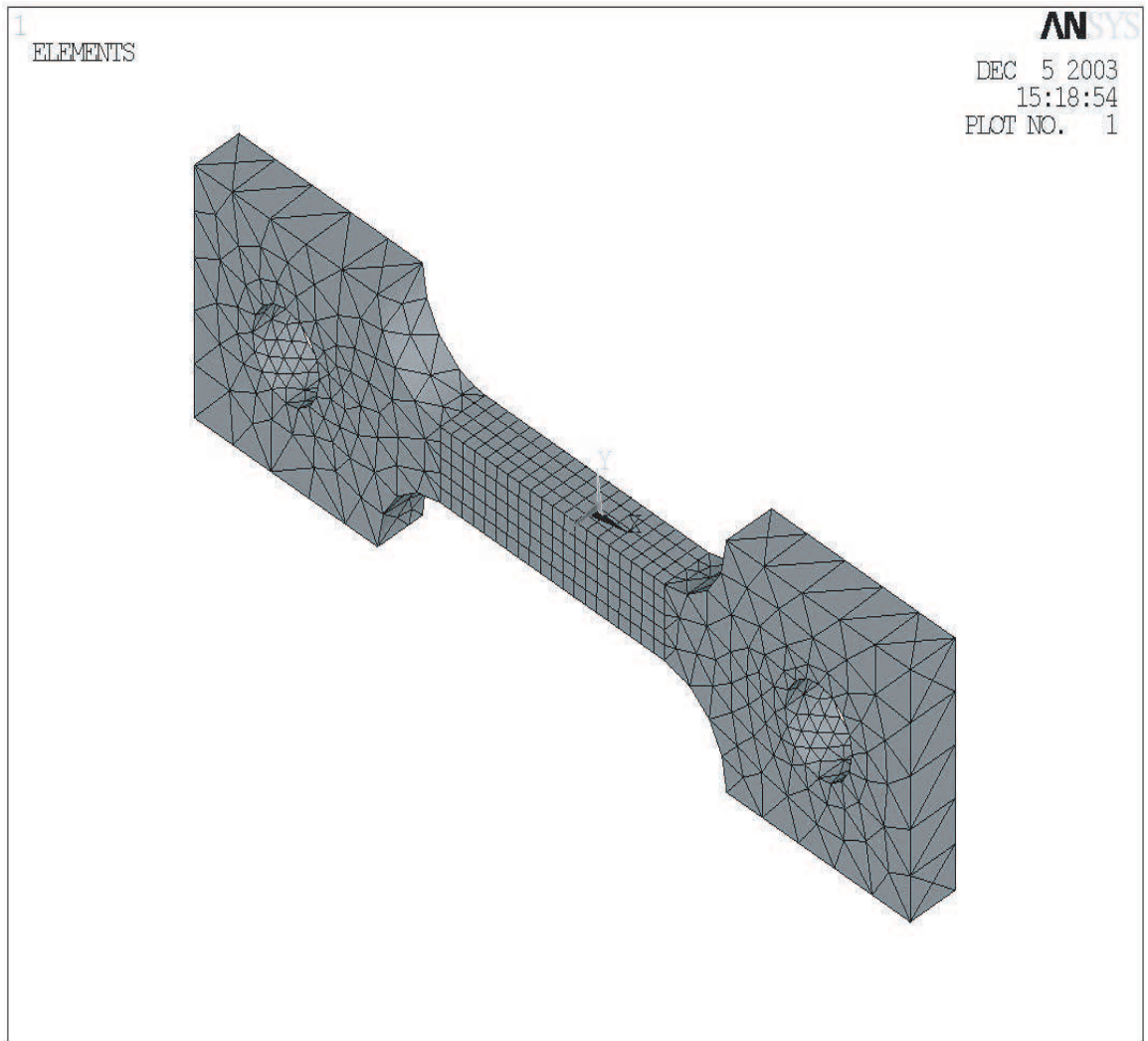
Figure 4.7: Model Meshing

4.3.3 Load Definition

The controlling parameter of the simulation is the displacement, and the nodal forces were extracted from the simulation. The gauge length of the specimen is taken to be 5 mm as shown on figure 4.4. The Model is prescribed to be fixed at the left edge of the left pin hole. The displacement boundary condition is prescribed at the right edge of the right pin hole as shown on figure 4.8. The displacement must be divided into small "load steps" in order for the algorithm to converge successfully. Figure 4.9 shows typical displacement load points on the engineering stress-strain curve. Each point on curve is a load point. Once the loads have been defined, the analysis can then be executed, and the engineering curve can then be extrapolated. To avoid local plastic deformation around the pin holes, the modulus of the two end sections with the pin holes have been raised to $2E20$ so all displacement loads can be directly transferred to the middle section.

4.3.4 Analysis Execution and Results

It normally takes thirty to forty minutes to complete ten to fifteen load steps of calculation. The results are then post-processed and analyzed. The nodal forces on the left of the pin holes are summed to obtained the engineering stress. The following chapter provides and discusses the results.
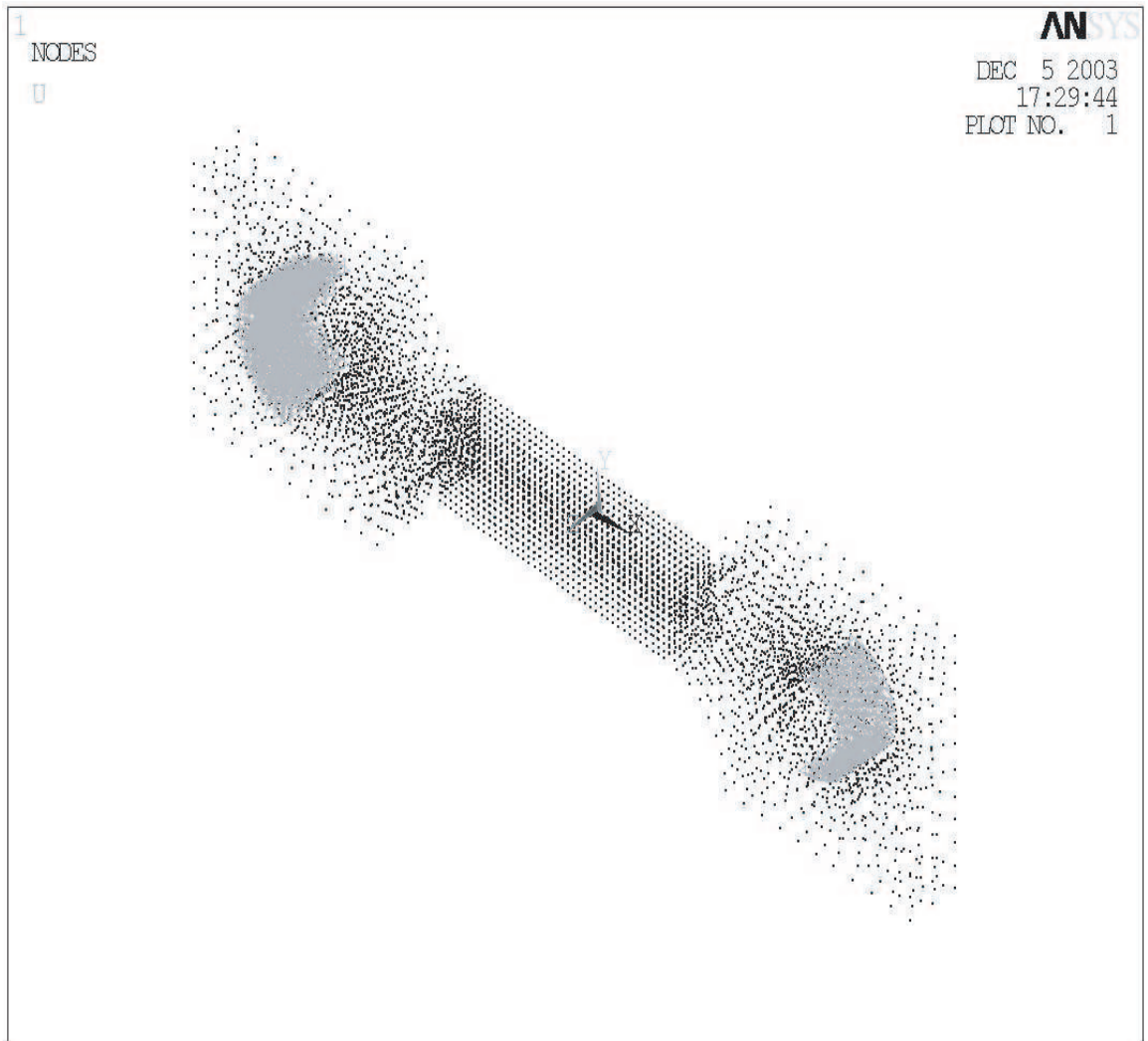
Figure 4.8: Boundary Conditions
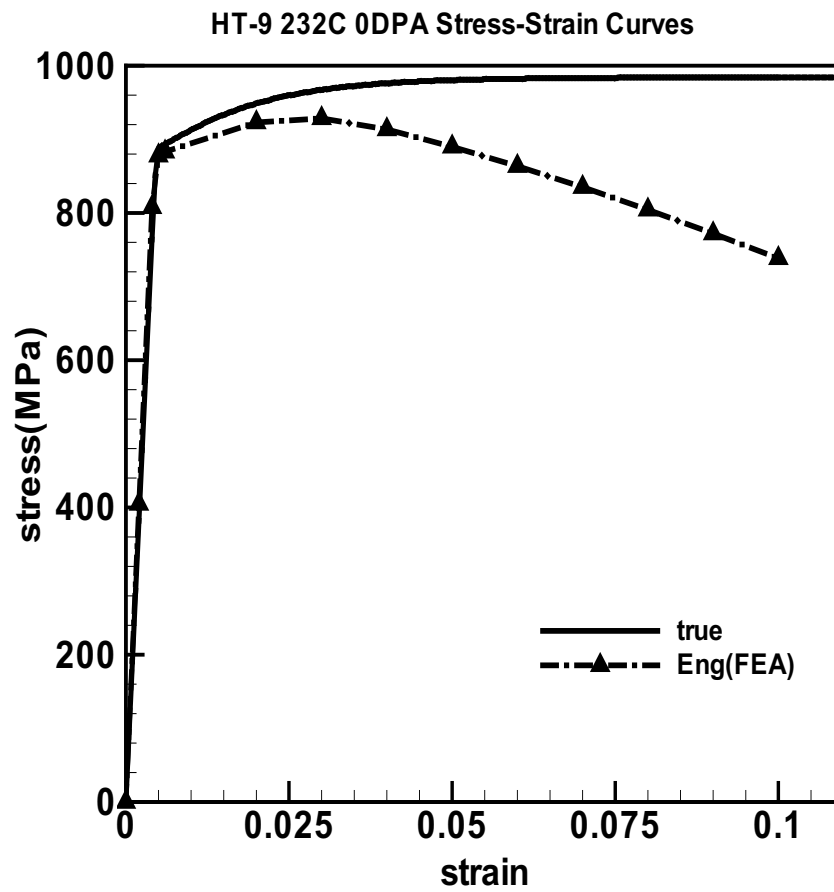
Figure 4.9: Load Steps shown on engineering stress-strain curves

CHAPTER 5

Results and Experimental Model Validation

The objective of this chapter is to show and discuss the results from implementing the Dislocation-based Constitutive Model, and from performing elasto-plastic Finite Element Analysis with the predicted true stress-strain curves. The results from the FORTRAN90 implementation will be shown and discussed first, followed by the Finite Element Analysis results, and a brief analysis of the plastic instability phenomenon.

5.1   FORTRAN90 Implementation Results

The model was executed for HT-9 and F82H at 232C, 450C, 550C, and 650C. There were total of eight input files created, and eight output files generated for each scenario. The sample input and output files are shown on appendix B and C. The total strain and stress are then plotted to obtain the true stress-strain curves for each scenario as shown on figure 5.1 to 5.8. The experimental results were obtained from [58] and [55], and have been plotted on figure 5.1 to 5.8 as well. However, only the yield strength, ultimate strength, uniform strain, and total strains were published on [58] and [55]. Therefore, the experimental fracture strength has been estimated.

It can be observed that the yield strength, Young's Modulus, the ultimate strength, and the elasto-plastic tangent from the FORTRAN implementation
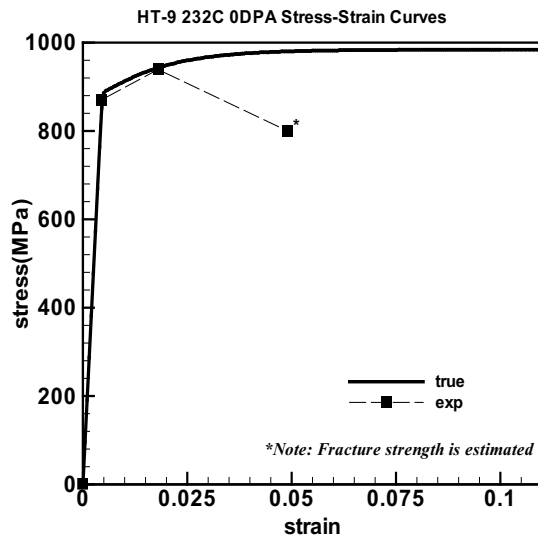
Figure 5.1: HT-9 232C 0DPA true and experimental stress-strain curves
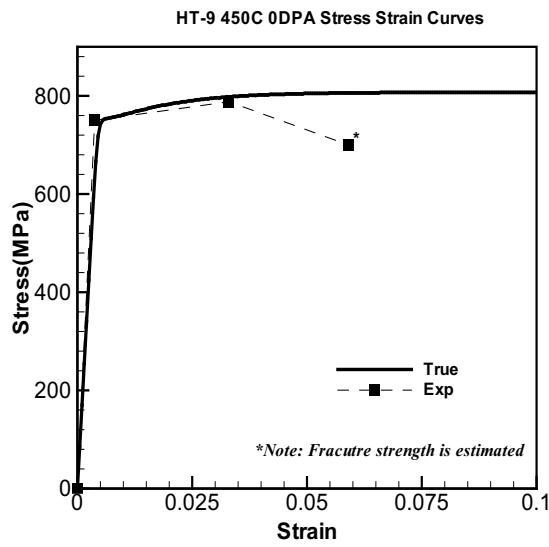
Figure 5.2: HT-9 450C 0DPA true and experimental stress-strain curves
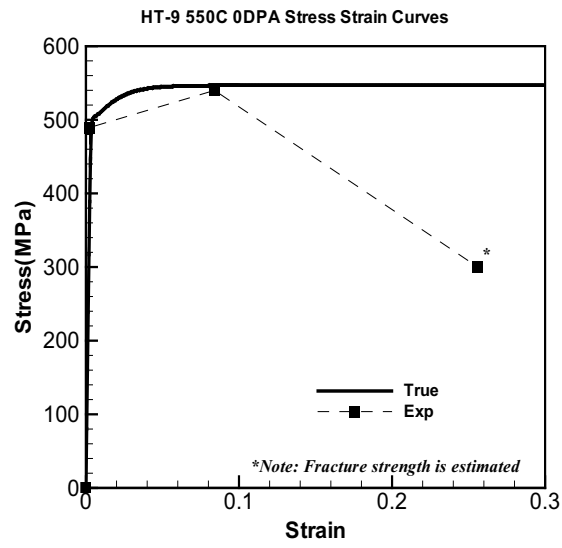
Figure 5.3: HT-9 550C 0DPA true and experimental stress-strain curves
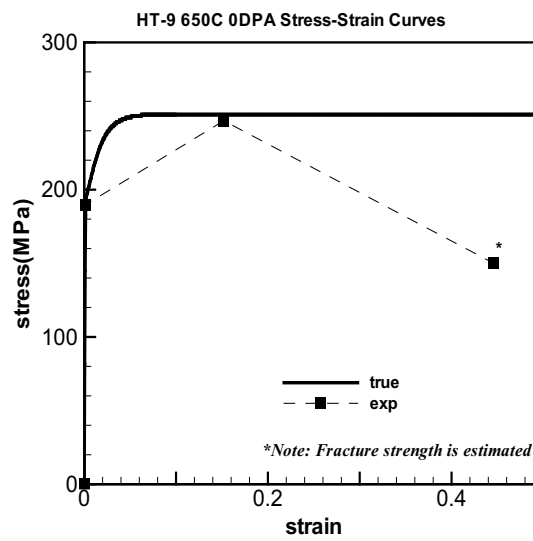
Figure 5.4: HT-9 650C 0DPA true and experimental stress-strain curves
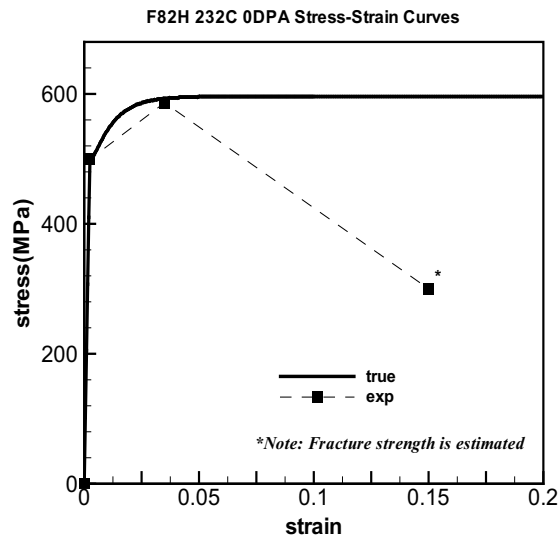
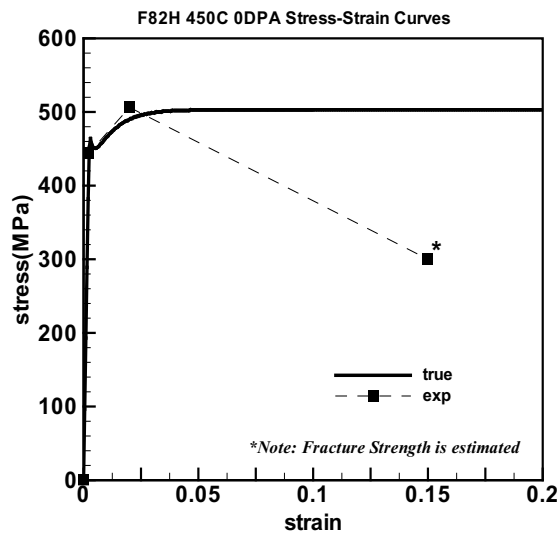Figure 5.5: F82H 232C 0DPA true and experimental stress-strain curves

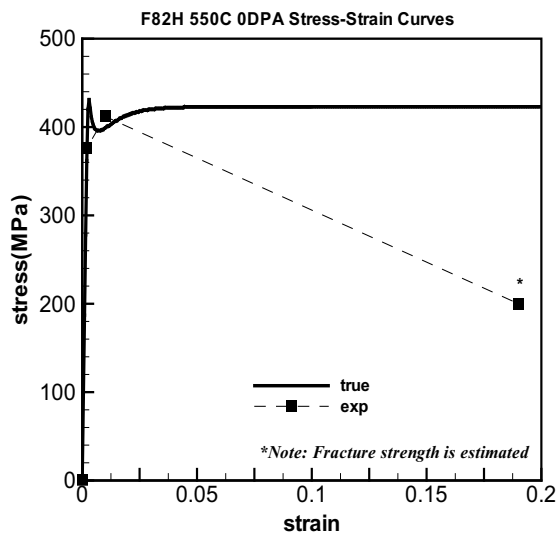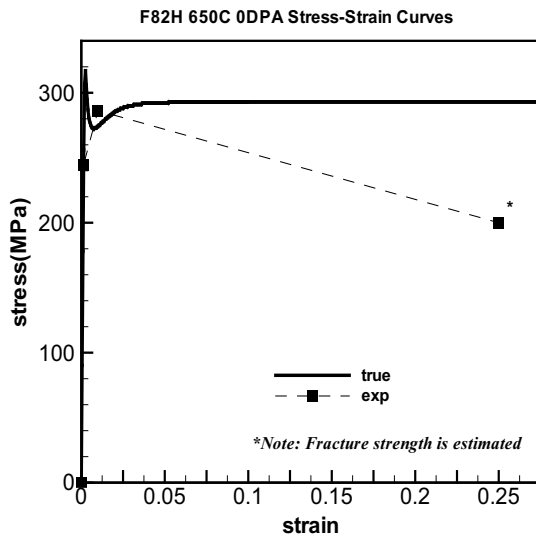Figure 5.6: F82H 450C 0DPA true and experimental stress-strain curves

Figure 5.7: F82H 550C 0DPA true and experimental stress-strain curves

Figure 5.8: F82H 650C 0DPA true and experimental stress-strain curves

matched quite well with experimental results. This result should be apparent since the model has been calibrated against experimental results.

5.2   Finite Element Analysis Results

The elasto-plastic Finite Element simulation results are listed in this section. The various deformation and uniaxial stress results will be shown and discussed. Figure 5.9 and 5.10 show a typical necked specimen simulated in ANSYS.
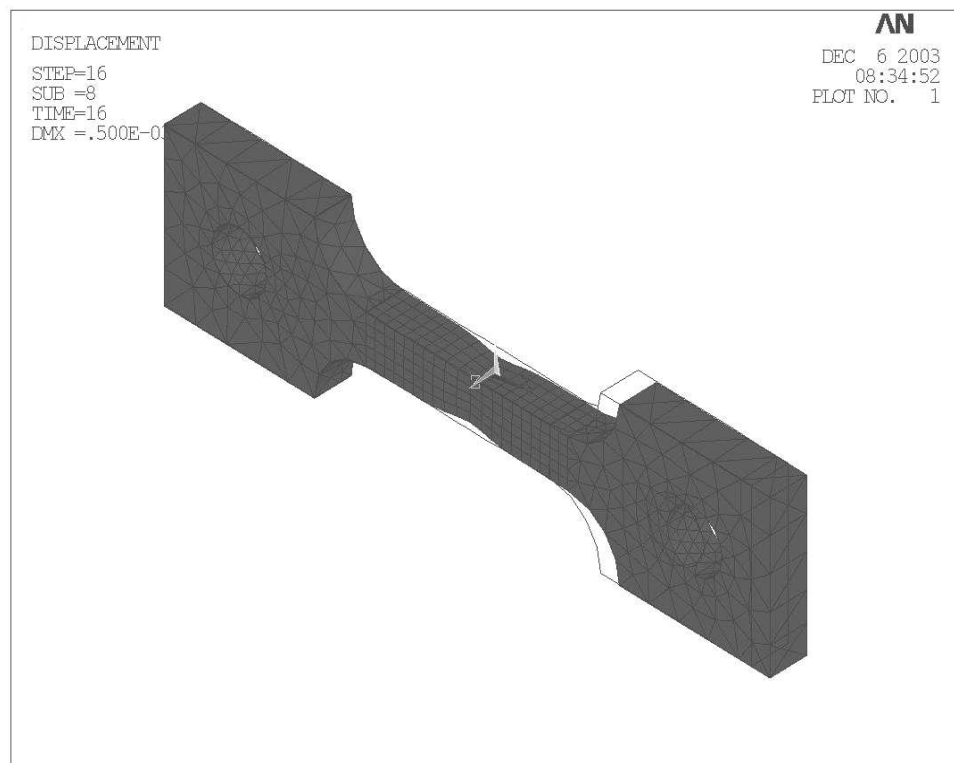
Figure 5.9: Typical Necked Sample

Figure 5.11 shows the displacement contour and figure 5.12 shows the uniaxial stress contour plot of a specimen. The displacement contour on figure 5.11 shows that all the displacements are experienced by the right side of the specimen.
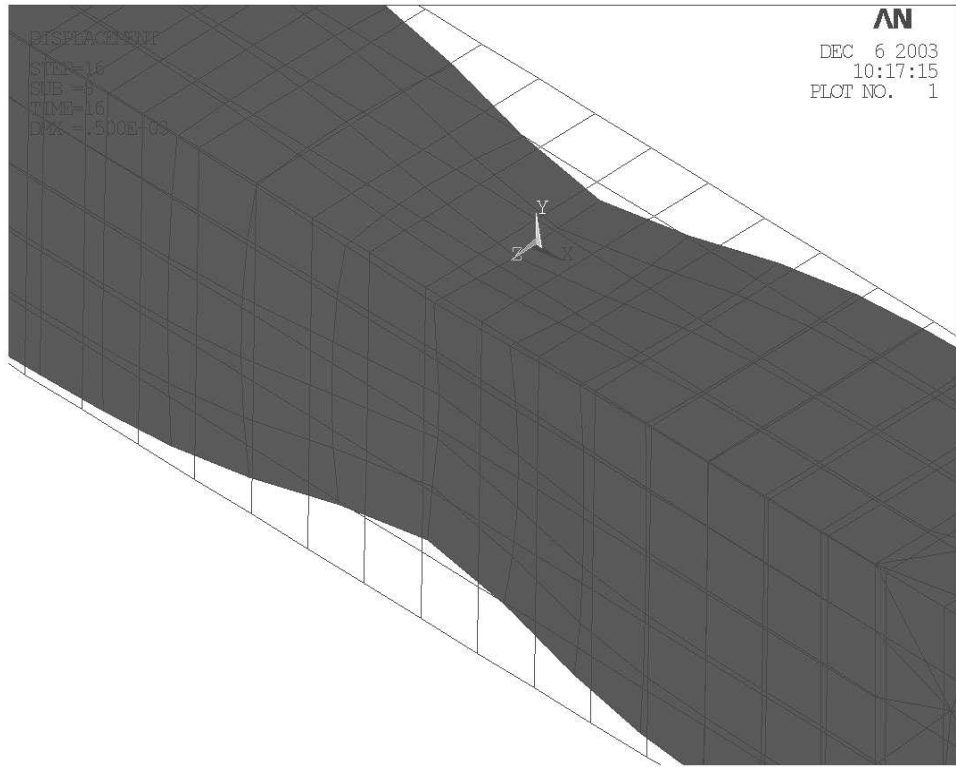
Figure 5.10: Typical Necked Sample Zoomed

This ensures that the accuracy of the experiments. The uniaxial stress contour on figure 5.12 shows that the stress is high in the middle of the specimen.
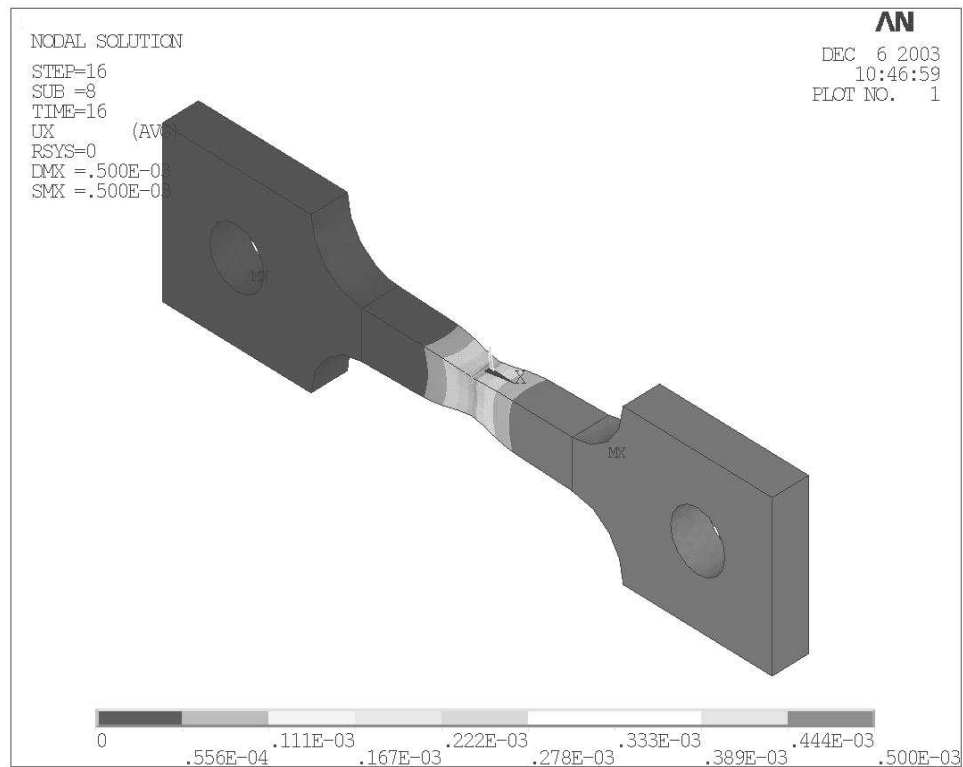

Figure 5.11: Displacement Contour Plot

As the previous chapter has discussed, the engineering stress strain curves can be measured from the nodal forces on the left pin hole. Figure 5.13 shows the True, Engineering Experimental, Engineering FEA stress-strain curves for HT-9 at 232C 0DPA, and figure 5.14 to 5.19 show the uniaxial stress contour at various stages of the stress strain curve. One can observe from figure 5.13 that the yield strength, young's modulus, ultimate strength, and elasto-plastic tangent predicted by ANSYS match quite well with the experimental value.

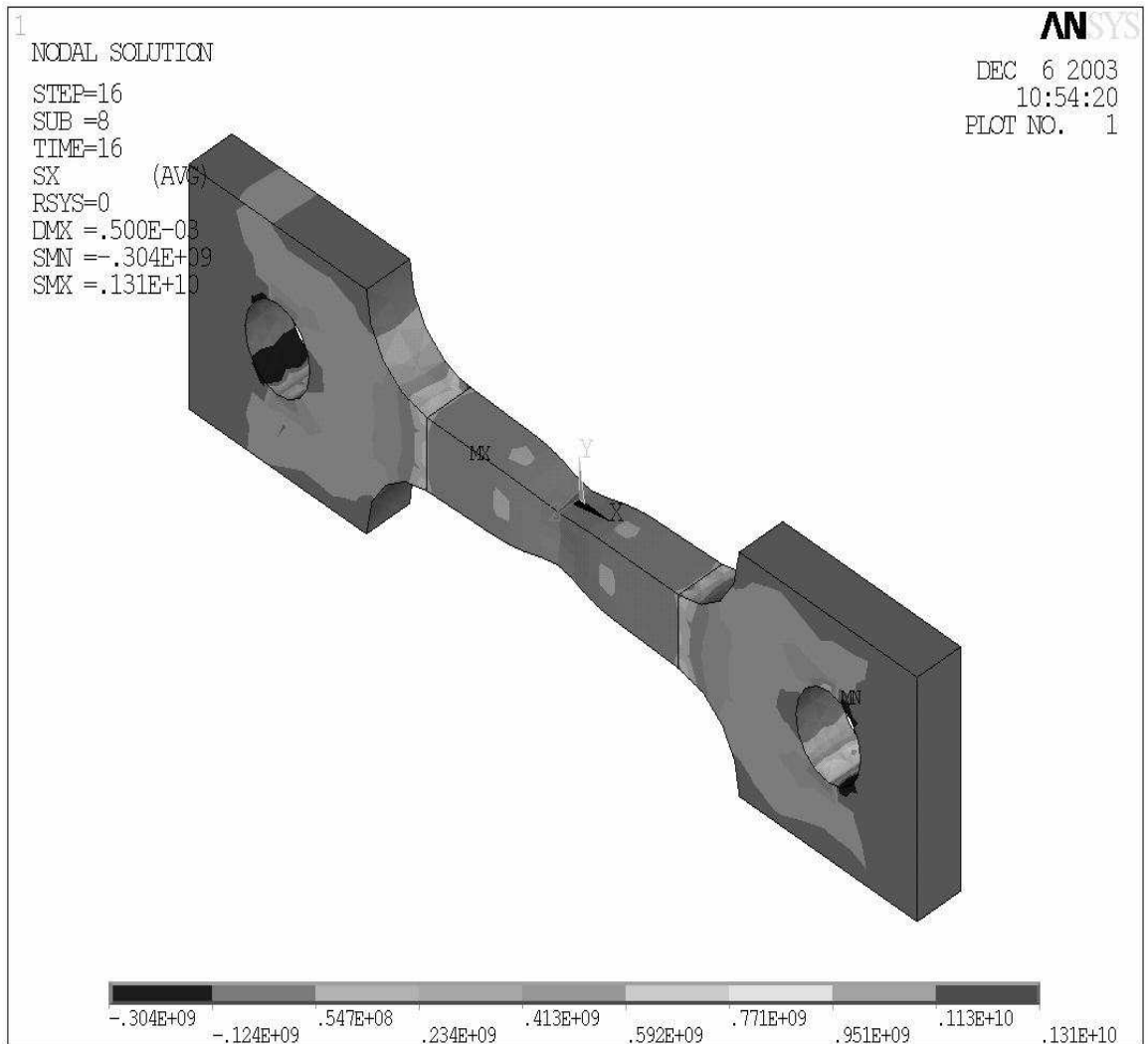Figure 5.20 to 5.34 show all the stress strain curves and the final deformation

60

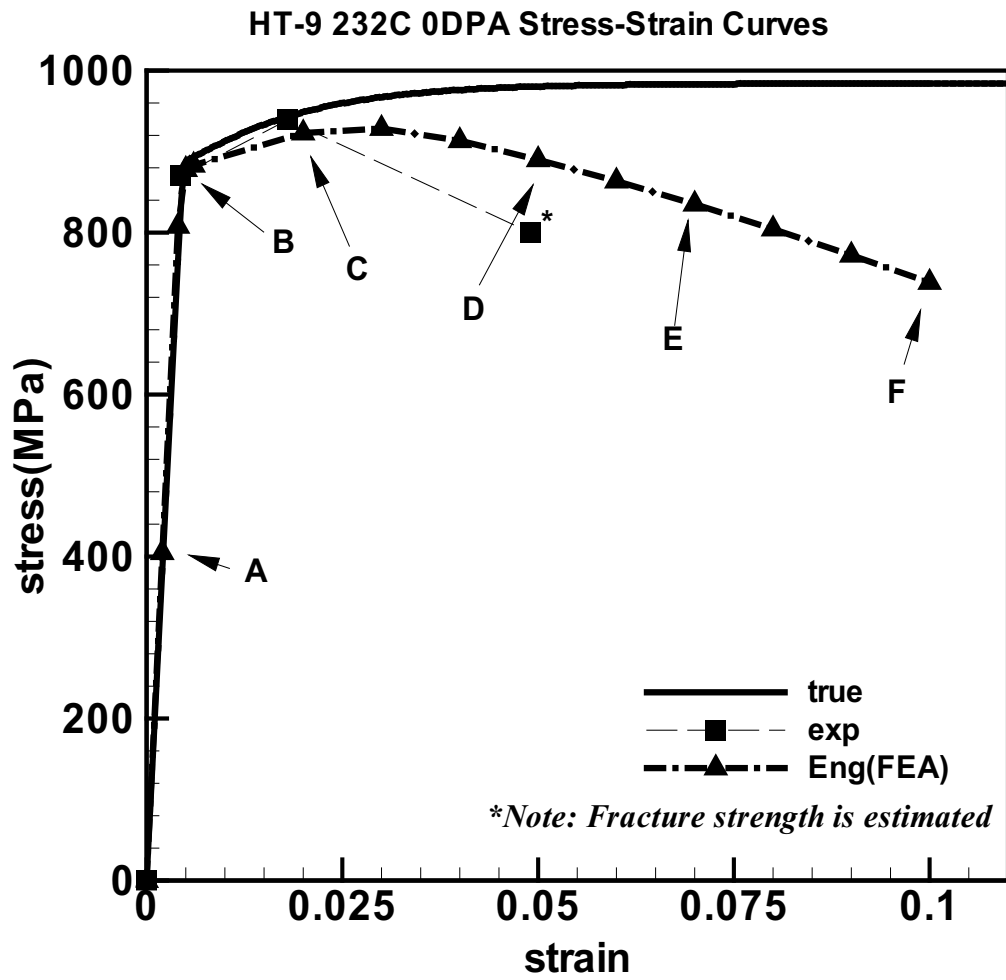Figure 5.12: Uniaxial Stress Contour Plot
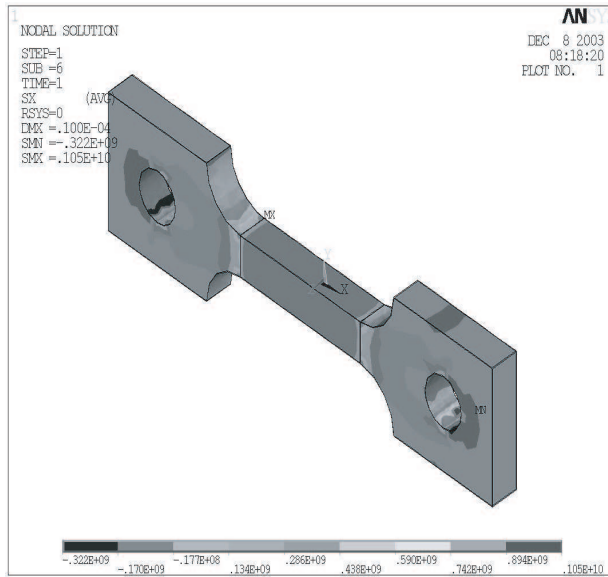
Figure 5.13: HT-9 232C 0DPA
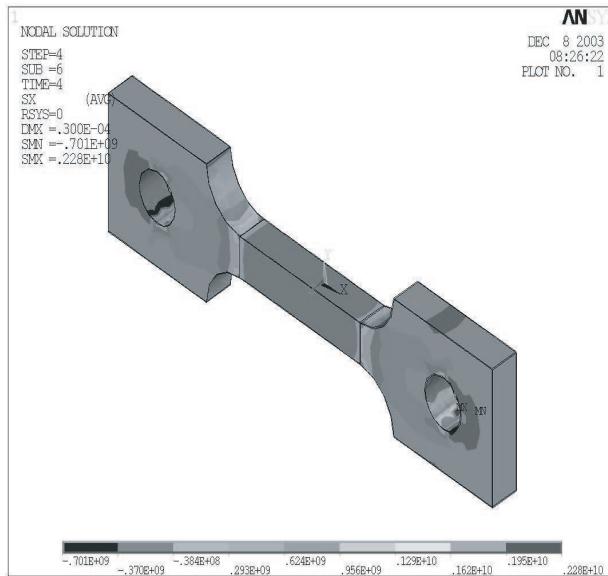
Figure 5.14: HT-9 232C 0DPA Stage A
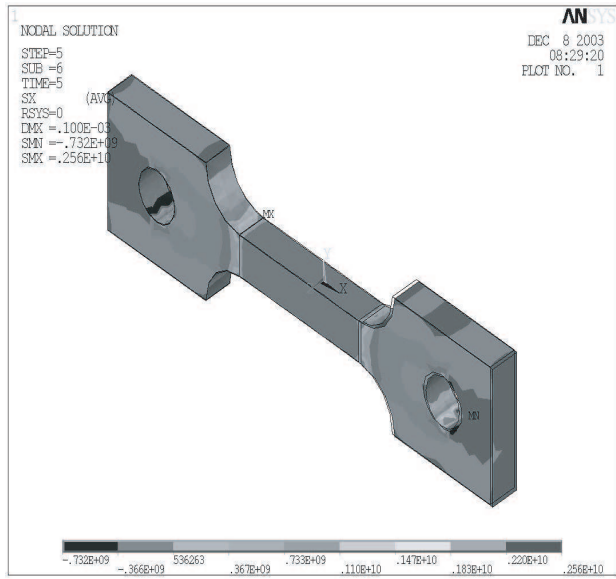

Figure 5.15: HT-9 232C 0DPA Stage B

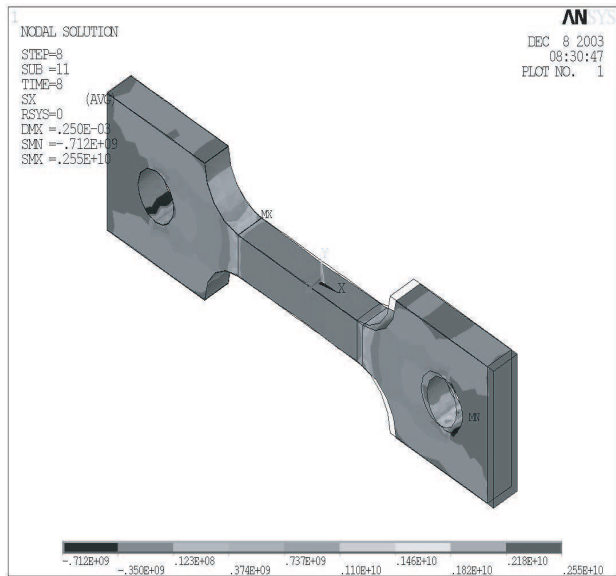Figure 5.16: HT-9 232C 0DPA Stage C
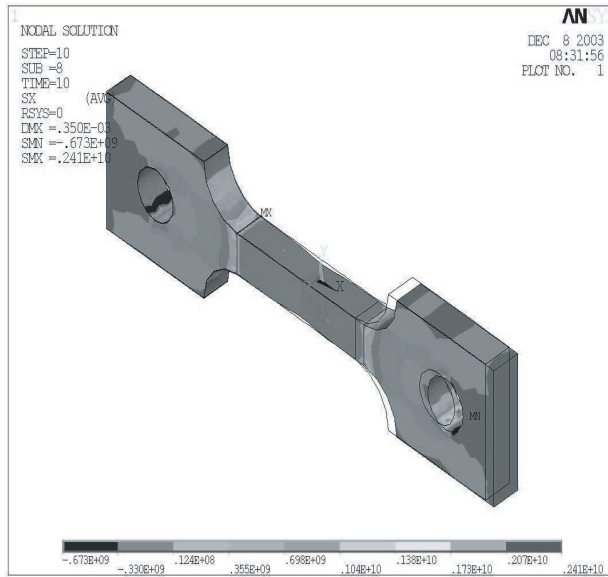

Figure 5.17: HT-9 232C 0DPA Stage D

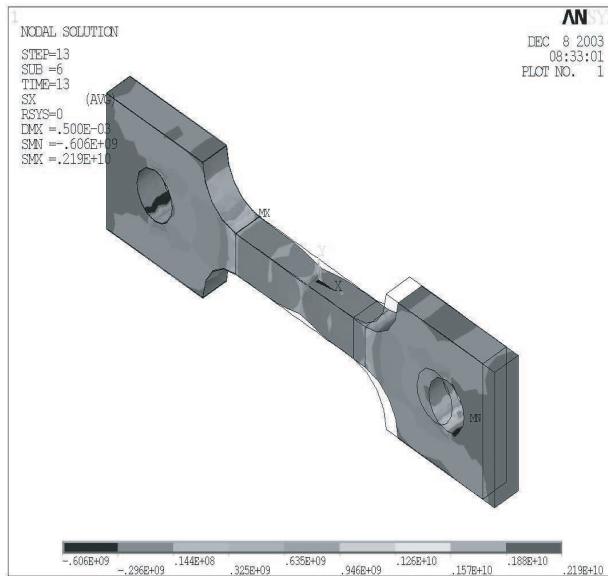Figure 5.18: HT-9 232C 0DPA Stage E

Figure 5.19: HT-9 232C 0DPA Stage F

for HT-9 and F82H at various temperatures. Again the ultimate and the yield strength from ANSYS match quite well with the experimental results except for HT-9 at 550C and 650C. This can be attributed to the large uniform elongation of the experimental stress strain curves. Further experimental studies at these temperatures should be conducted to ensure the accuracy of the uniform elongations.

Yield drop can also be observed from F82H 450C to F82H 650C. The initial dislocation density for F82H are two orders of magnitude smaller than HT-9. Further investigations should be pursued to describe the phenomenon for explaining yield drop occurring at alloys with lower dislocation densities.

Figure 5.20: HT-9 232C 0DPA stress-strain curves

Figure 5.21: HT-9 232C 0DPA Final Displacement

Figure 5.22: HT-9 450C 0DPA stress-strain curves

Figure 5.23: HT-9 450C 0DPA Final Displacement
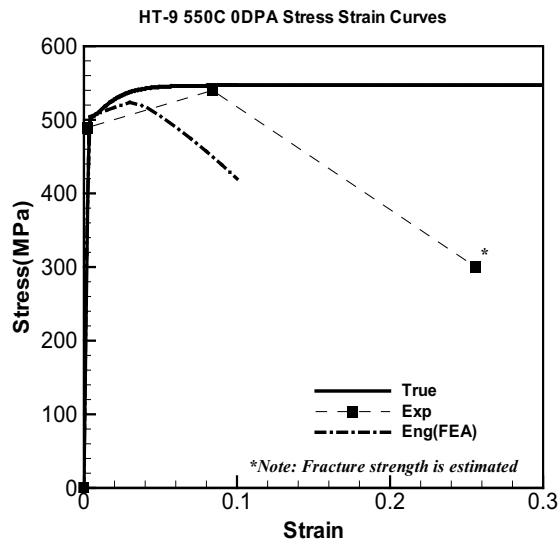
Figure 5.24: HT-9 550C 0DPA stress-strain curves
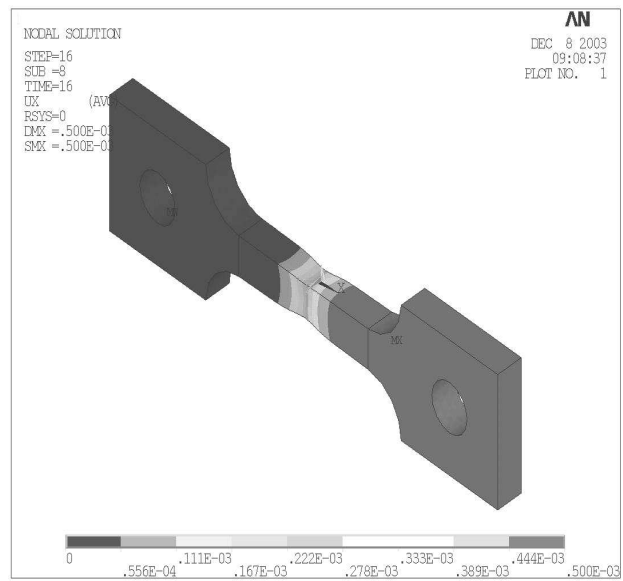
Figure 5.25: HT-9 550C 0DPA Final Displacement

69
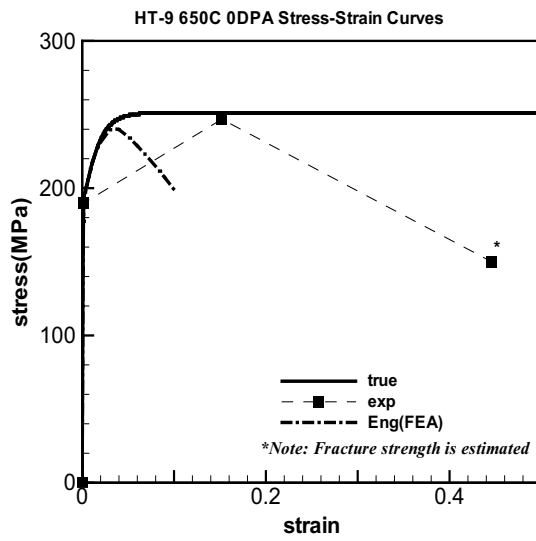
Figure 5.26: HT-9 650C 0DPA stress-strain curves
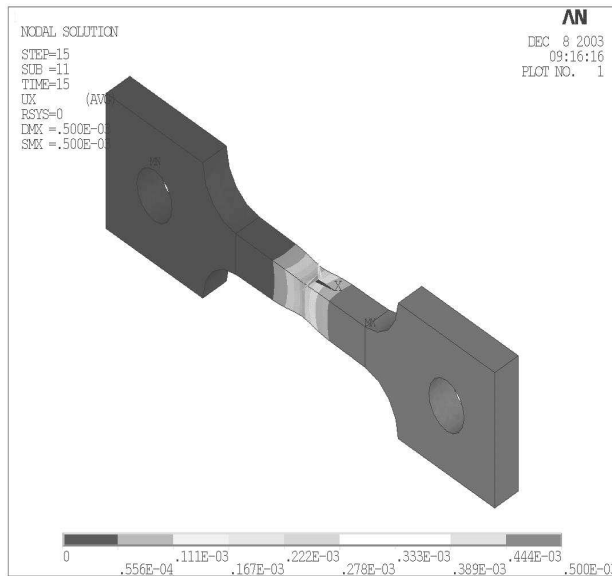
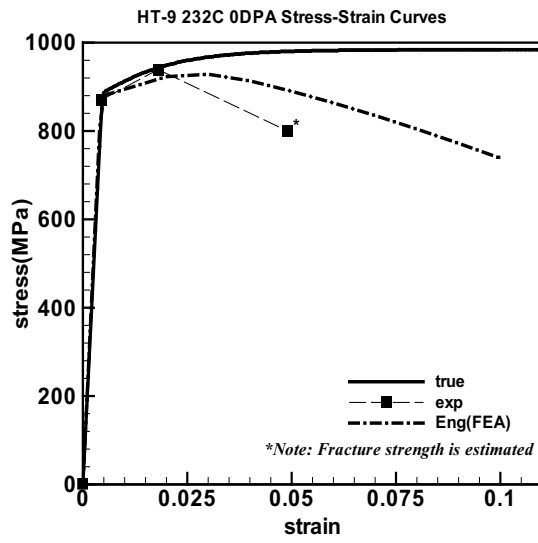Figure 5.27: HT-9 650C 0DPA Final Displacement
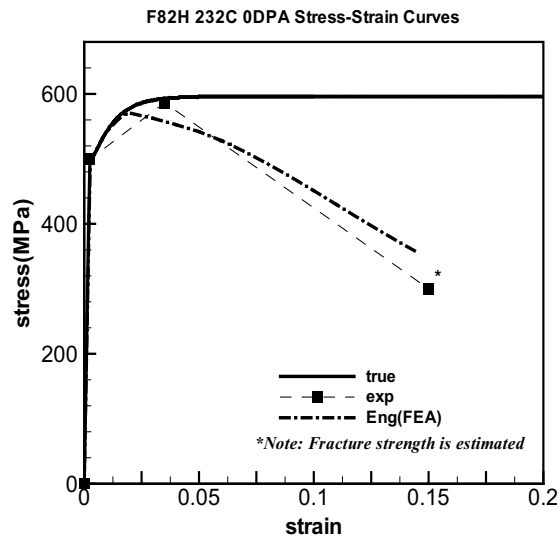
Figure 5.28: F82H 232C 0DPA stress-strain curves
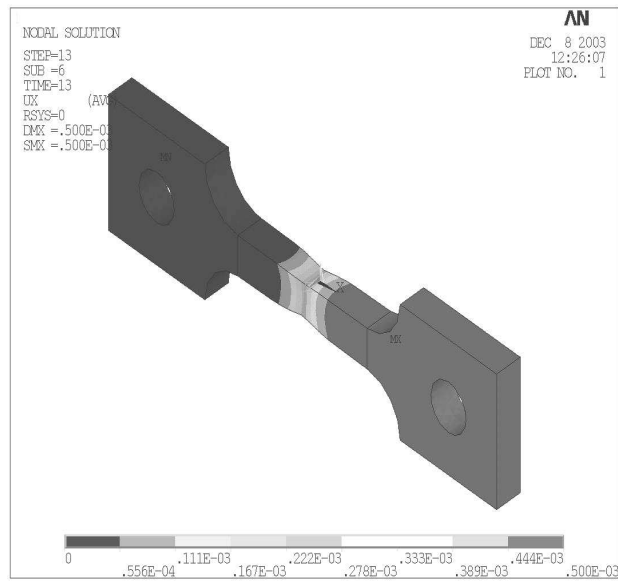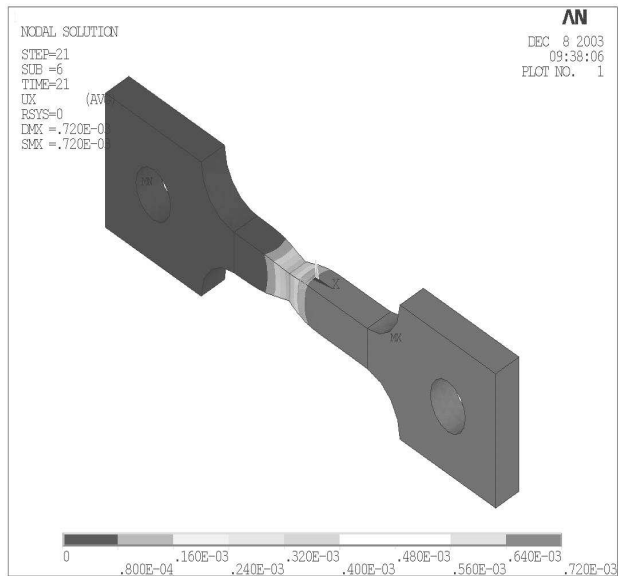

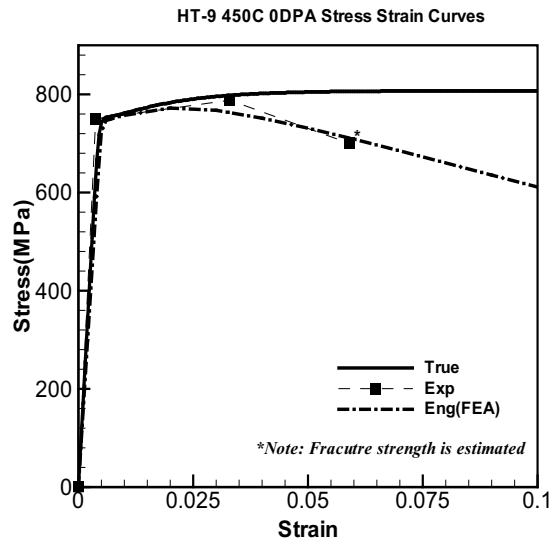Figure 5.29: F82H 232C 0DPA Final Displacement
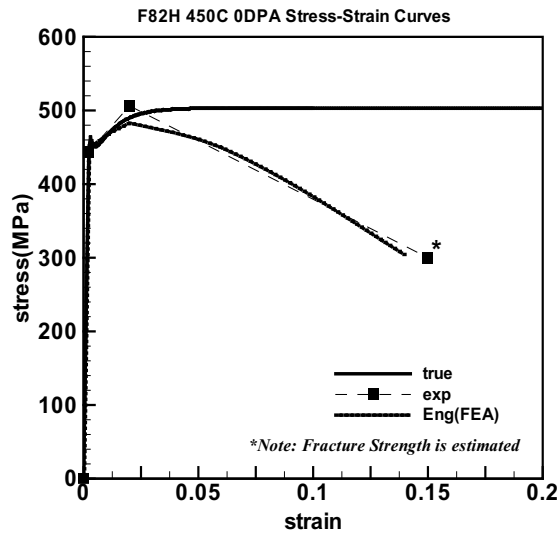
Figure 5.30: F82H 450C 0DPA stress-strain curves
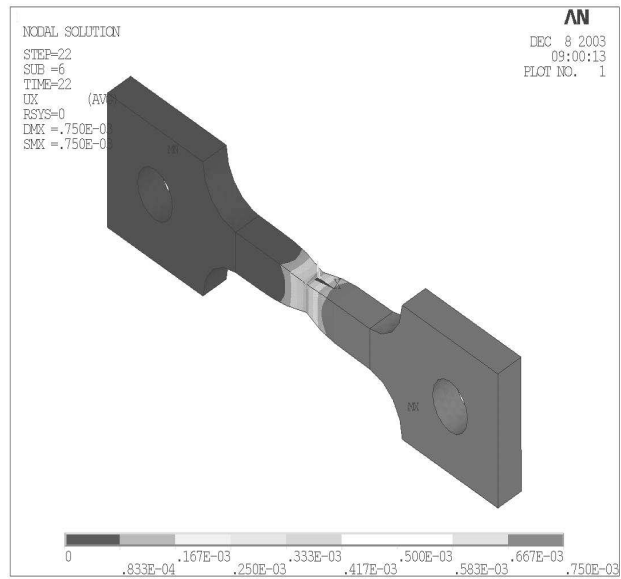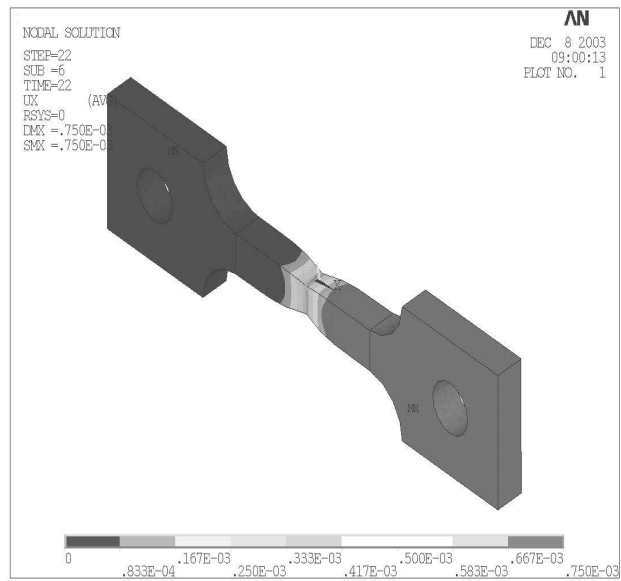

Figure 5.31: F82H 450C 0DPA Final Displacement
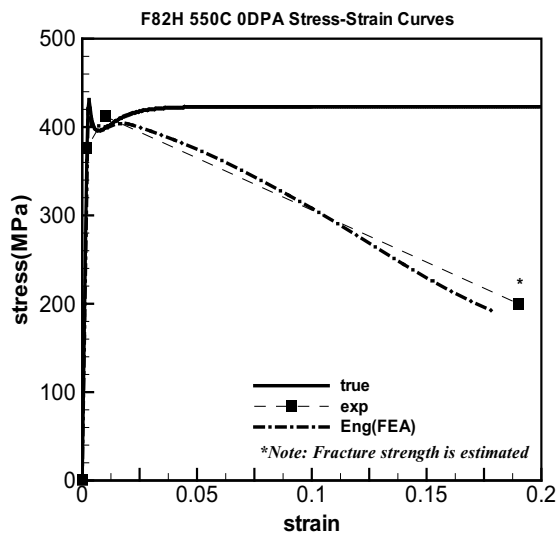
Figure 5.32: F82H 550C 0DPA stress-strain curves
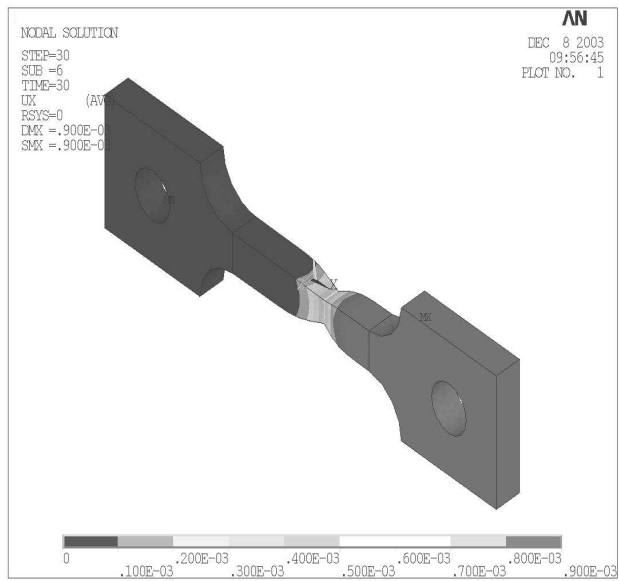
Figure 5.33: F82H 550C 0DPA Final Displacement

73
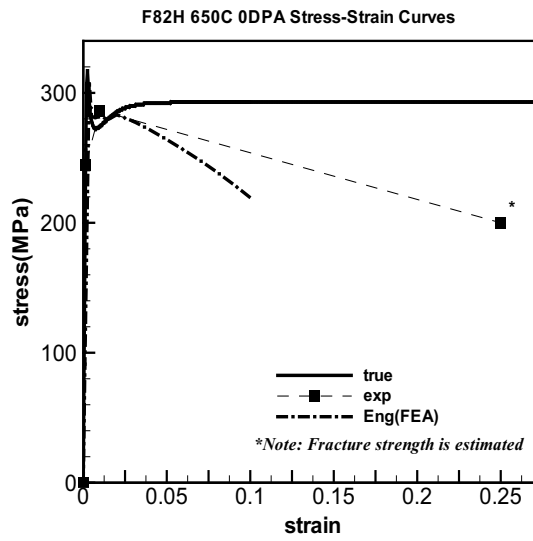
Figure 5.34: F82H 650C 0DPA stress-strain curves
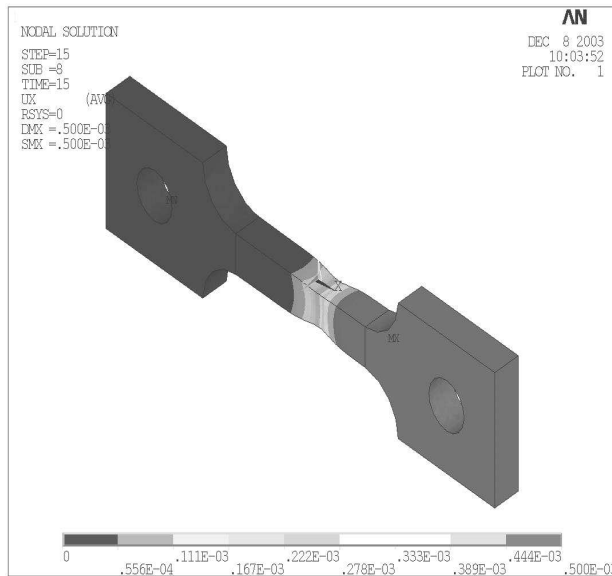
Figure 5.35: F82H 650C 0DPA Final Displacement

Figure 5.36 and 5.38 show the details of the local yield drop just after the yield strength for F82H operating at 450C, 550C, and 650C. Local yield drop can be observed from post-irradiated F82H and HT-9. Figure 5.36 to 5.38 show that this phenomenon can be simulated via Finite Element Analysis. The exact cause of this phenomenon should still be further investigated.
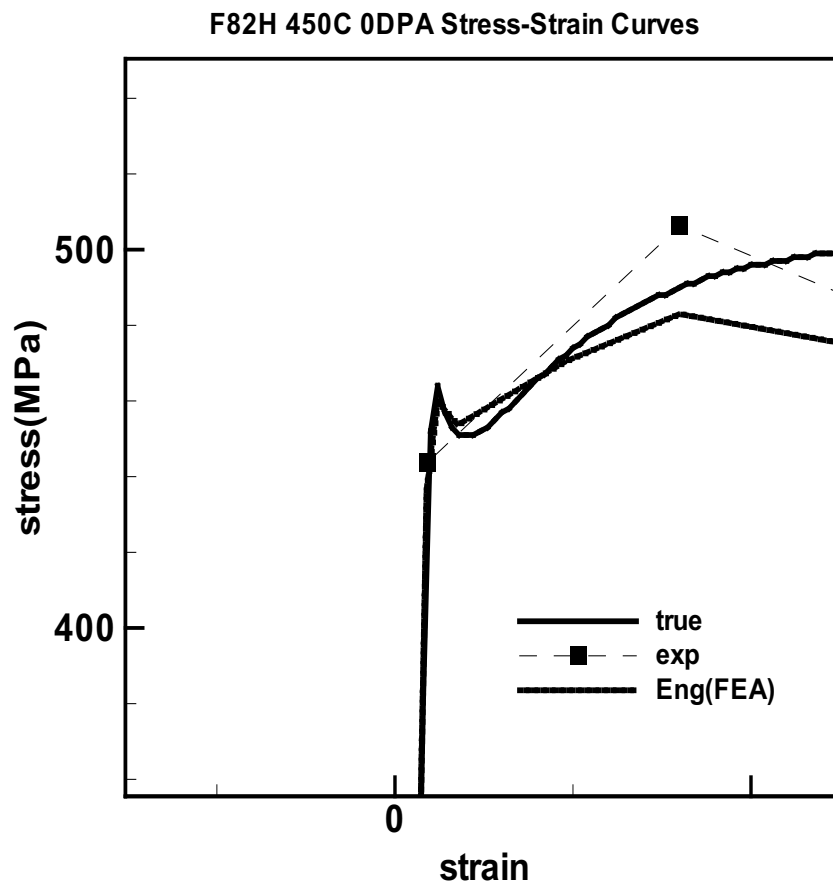
Figure 5.36: F82H 450C 0DPA Yield Drop
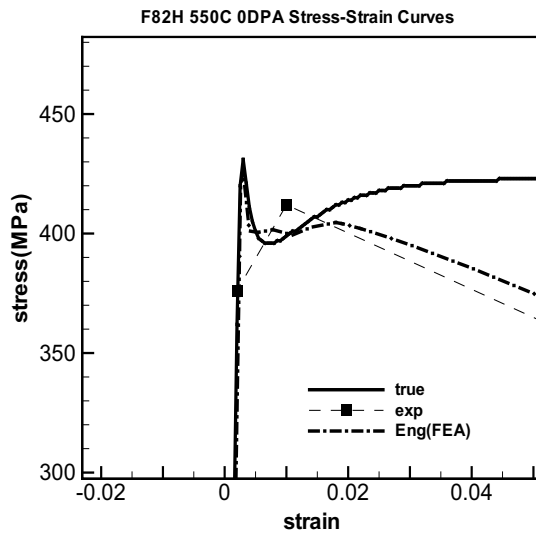
Figure 5.37: F82H 550C 0DPA Yield Drop
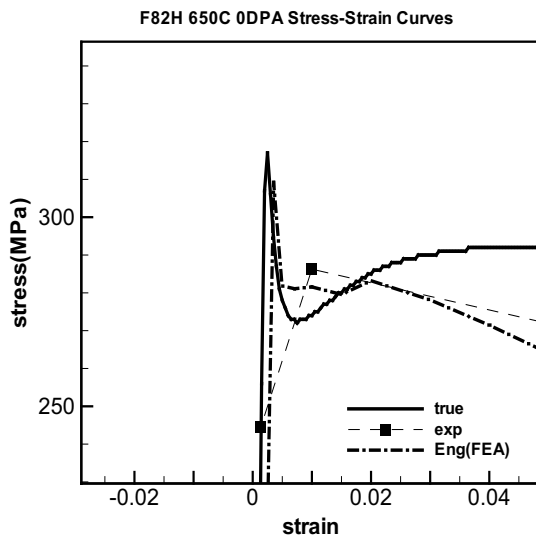
Figure 5.38: F82H 650C 0DPA Yield Drop

5.3 Brief Analysis of Plastic Instability

The phenomenon of plastic instability, or visibly observed as necking, is the phenomenon that commences from reaching of the ultimate strength until fracture. During this stage, plastic deformation becomes much more rapid, and large deformation of necking can be observed. By plotting the mobile dislocation density on the stress-strain curves. One can obtain an insight on how mobile dislocations relate to the commence of plastic instability.

It can be observed from figure 5.39 to 5.41 that the mobile dislocation density reaches a steady state near the commencement of plastic instability. One can thus postulate that it is due to the dislocation production reaching a steady state, that the hardening ceases and plastic instability commences. Since this is only a very brief treatment of this subject, further studies would be required to understand the causes of this phenomenon.
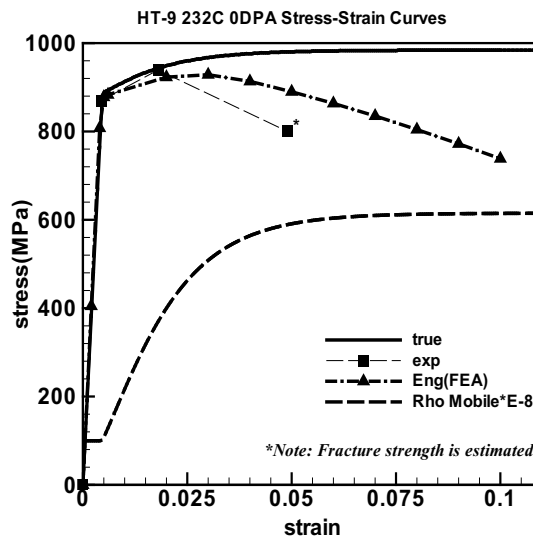
Figure 5.39: HT-9 232C 0DPA stress-strain curves with Mobile Dislocation
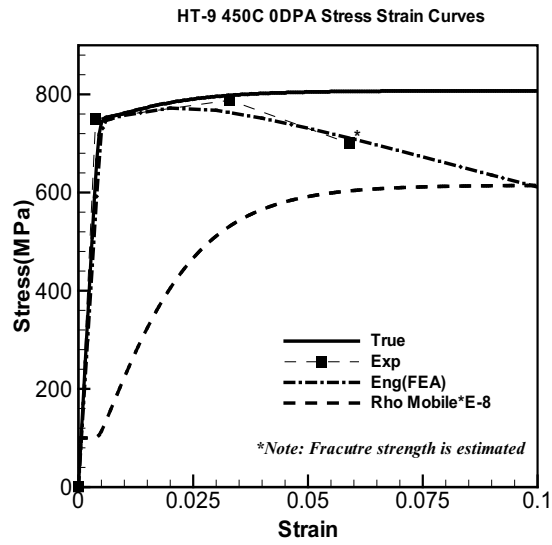
Figure 5.40: HT-9 450C 0DPA stress-strain curves with Mobile Dislocation
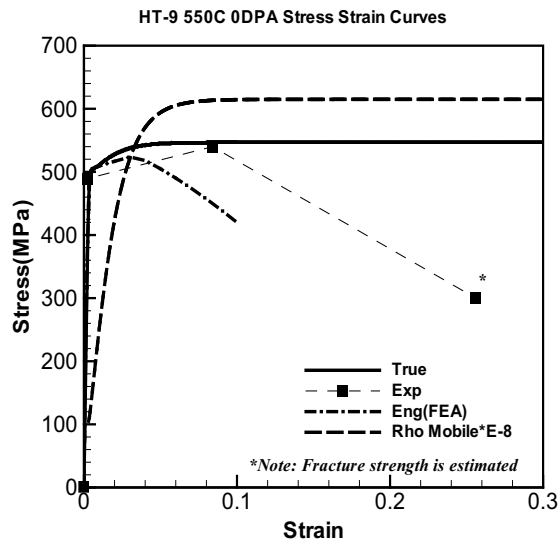
Figure 5.41: HT-9 550C 0DPA stress-strain curves with Mobile Dislocation

CHAPTER 6

Conclusions

The Ghoniem-Matthews-Amodeo Creep Model has been extended to a Stress-strain Constitutive Model. The Model has been computationally implemented and calibrated by microstructure parameters for ferritic-martensitic alloys HT-9 and F82H at a wide range of temperatures. True stress-strain curves predicted by the model has been incorporated into a commercial Finite Element Package (ANSYS) to perform elasto-plastic analysis on a dog-bone tensile specimen. Engineering stress-strain curves were obtained from the Finite Element Analysis for HT-9 and F82H at 232C, 450C, 550C, and 650C. These curves were then compared with experimentally obtained data, and the results have been shown in chapter 5.

From implementing the Dislocation-based Models, and observing the Finite Element Analysis Results, a number of conclusions can be drawn as the following.

- First, the Ghoniem-Matthrews-Amodeo Creep Model has been shown to be able to be extended to a Constitutive Model.

- Second, it has been shown that it is possible to calibrate the extended model by microstructure parameters so true stress-strain curves for HT-9 and F82H at various temperatures can be predicted.

- Third, the calibrated stress-strain curves can be successfully implemented in a commercial Finite Element Package such as ANSYS to analyze elasto-

plastic material deformations.

- Fourth, the plastic instability and necking effect can potentially be a function of the rate of production of dislocations

The first conclusion can be drawn because true stress-stress curves can be obtained from the extended model. A true stress-strain curve can be obtained from solving equations from section 3.9 on page 34. The values of the applied stress, σ and the input total strain ε are plotted to obtain the true stress-strain curves. Figure 4.3 on page 43 shows the typical true stress strain curve. This technique is different from a constitutive model that evolves over strain, such as the KM Model shown earlier. The results however, showed very close resemblance to the actual steel alloy stress-strain behaviors as one can see from figure 5.20 to 5.38 from page 67 to page 76.

The second conclusion can be drawn because critical features on the true stress-strain curve can be calibrated via microstructure parameters. These critical features include the yield strength, ultimate strength, Young's Modulus, and the elasto-plastic tangent. The calibration parameters have been summarized on figure 4.5 and 4.6 on page 45. It can be observed that the yield strength is the most sensitive to initial dislocation density $\rho(0)$, activation volume Ω, precipitate parameters N_p and r_p, and dislocation vibrational frequency ν_d. It is well known that the yield strength can be calibrated against the square root of the dislocation density. The effects of precipitates and dislocation vibrational frequency are also well known. However, the effect of activation volume Ω is less well known. From [30], the effect of activation volume can be related to the activation energy U as the following,

$$U = U_0 - v(\tau - \tau_G) \tag{6.1}$$

80

where U_0 is the local energy barrier, v is the activation volume, and τ and τ_G are the flow stress and the temperature independent component of the flow stress. If the activation volume is increased, then less activation energy would be require to initiate the flow stress. This can possibly explain the validity of using activation volume as a calibrating parameter. However, further study should be pursued to ensure the validity of this calibrating parameter. The hardening rate can be calibrated by the critical dislocation spacing parameter δ due to dynamic recovery. The value used for this parameter is approximately 40-60 nm. This match the results published by Essmann et al [14] quite well, which is 50-500 nm for screw and 1.6 nm for edge dislocations(in copper).

The third conclusion can be drawn because the engineering stress-strain curves obtained from FEA show reasonable match to the experimental values. The yield and ultimate strength obtained from ANSYS as shown on figure 5.20 to 5.38 from page 67 to 76 correspond quite well with experimental results. The effect of necking and local strain softening can also be observed as shown on numerous figures in chapter 5.

The fourth conclusion can be drawn by observing figure 5.39 to 5.41 on chapter 5. As the previous chapter had discussed, plastic instability can be observed when mobile dislocation production reaches a steady state. Further studies have to be done in order to strength this conclusion. However, one should be able to safely state that the plastic instability is related to the production and annihilation of dislocations.

The overall results of implementing the dislocation-based model seem promising. However, a number of areas can still be further investigated to ensure the validity of this model. Some of the areas include the validity of the calibration parameters and values, and the experimental value validations. The calibration parameters such as the activation volume should be further investigated to prove its validity

for use in calibration. The experimental results should also be further validated since it dictates the values used for calibration. Actual tensile experiments should be conducted to provide better experimental values in calibrating the stress strain curves.

APPENDIX A

Dislocation-based Constitutive Model
FORTRAN90 Code

```fortran
PROGRAM MAIN


IMPLICIT REAL*8 (A-H, O-Z)
EXTERNAL DIFFUN, JAC
  INTEGER  IOPT, IOUT, ISTATE, ITASK, ITOL, IWORK(30), LIW, LRW,
 1          MF, NEQ, NUM
  DOUBLE PRECISION  ATOL(6), RTOL, RWORK(437), T, TOUT, Y(6),
 1 YDOT(6), ETOT, DUMMY(3)
CHARACTER*8 INP1, METAL

  PRINT *, 'Constant strain rate test (Y/N)?'
  READ *, INP1
  IF (INP1 .EQ. 'Y') THEN
    NEQ = 6
    PRINT *, 'Please enter time step (hours)'
    READ *, TIME
```

```fortran
      OPEN(4, FILE='INPUT.txt')
      READ (4, *) TFINAL, EDOT, METAL, DUMMY(1), DUMMY(2),
1                 DUMMY(3)
      CLOSE (4, STATUS='KEEP')
     ELSE
       NEQ = 5
       PRINT *, 'Please enter time step (hours)'
       READ *, TIME
       OPEN(4, FILE='INPUT.txt')
       READ (4, *) TFINAL
       CLOSE (4, STATUS='KEEP')
      END IF


!       OPEN(4, FILE='INPUT.txt') !    READ (4, *) TFINAL, EDOT,
CDUMMY, DUMMY(1), DUMMY(2),
 !   1 DUMMY(3)
!    READ (4, *) TFINAL !    CLOSE (4, STATUS='KEEP')


      TFINAL = TFINAL*3600


    IF (METAL.EQ.'F82H') THEN
      Y(1) = 1.D-4
       Y(2) = 1.D12
       Y(3) = 1.D11
      Y(4) = 1.D11
      Y(5) = 1.D-3
      Y(6) = 1.D-6/1.602D-19
```

84

```fortran
      ELSE
         Y(1) = 1.D-4
            Y(2) = 1.D10
            Y(3) = 1.D9
         Y(4) = 1.D9
         Y(5) = 1.D-3
         Y(6) = 1.D-6/1.602D-19
      END IF

            T = 0.D0
            TOUT = TIME*3600
         NUM=NINT((TFINAL-T)/TOUT)
         ITOL = 2
            RTOL = 1.D-4
            ATOL(1) = 0.D-8
            ATOL(2) = 0.D-8
            ATOL(3) = 0.D-8
         ATOL(4) = 0.D-8
         ATOL(5) = 0.D-8
         ATOL(6) = 0.D-8
            ITASK = 1
            ISTATE = 1
            IOPT = 0
            LRW = 437
            LIW = 30
            MF = 22
         %OPEN (10, FILE='OUTPUT.txt')
```

```
      IF (NEQ .EQ. 5) WRITE (10, 11) 'TIME(HR)', 'P_STRAIN',
   1 'RHOM', 'RHOS', 'RHOB', 'RADIUS'
      IF (NEQ .EQ. 6) WRITE (10, 13) 'TIME(HR)', 'P_STRAIN',
   1 'RHOM', 'RHOS', 'RHOB', 'RADIUS', 'STRESS', 'TOT_STRAIN'
11    FORMAT(/, 1X, A8, 6X, A8, 10X, A8, 12X, A8, 12X, A8, 14X, A8,/)
13    FORMAT(/, 3X, A8, 6X, A8, 10X, A8, 12X, A8, 12X, A8, 14X, A8,
   1  10X, A10, 14X, A10/)


      OPEN (11, FILE='INFO.txt')
      IF (NEQ .EQ. 5) WRITE (11,12) 'TIME(HR)', 'YDOT(1)',
   1    'YDOT(2)', 'YDOT(3)', 'YDOT(4)', 'YDOT(5)'
12    FORMAT(/, 8X, A8, 8X, A10, 8X, A13, 8X, A10, 10X, A10,
   1       10X, A10/)
      IF (NEQ .EQ. 6) WRITE (11,16) 'TIME(HR)', 'YDOT(1)',
   1    'YDOT(2)', 'YDOT(3)', 'YDOT(4)', 'YDOT(5)', 'YDOT(6)'
16    FORMAT(/, 8X, A8, 8X, A10, 8X, A13, 8X, A10, 10X, A10,
   1       10X, A10, 10X, A10/)
      DO 40 IOUT = 1,NUM-1
        CALL DLSODE (DIFFUN, NEQ, Y, T, TOUT, ITOL, RTOL, ATOL, ITASK,
   1                 ISTATE, IOPT, RWORK, LRW, IWORK, LIW, JEX, MF)
      IF (NEQ .EQ. 5) THEN
       WRITE (10, 20) T/3600, Y(1), Y(2), Y(3), Y(4), Y(5)
       PRINT 20,T/3600, Y(1), Y(2), Y(3), Y(4), Y(5)
20       FORMAT(1X, D12.4, 6D20.8)
       CALL DIFFUN(NEQ,T,Y,YDOT)
       WRITE (11,14) T/3600, YDOT(1), YDOT(2), YDOT(3), YDOT(4),
   1      YDOT(5)
```

86

```fortran
14      FORMAT(6D20.8)
        END IF


    IF (NEQ .EQ. 6) THEN
     ETOT = EDOT * T
     WRITE (10, 21) T/3600, Y(1), Y(2), Y(3), Y(4), Y(5),
  1      Y(6)*1.602D-19, ETOT
     PRINT 21,T/3600, Y(1), Y(2), Y(3), Y(4), Y(5), Y(6), ETOT
21       FORMAT(1X, D12.4, 7D20.8)
     CALL DIFFUN(NEQ,T,Y,YDOT)
     WRITE (11,15) T/3600, YDOT(1), YDOT(2), YDOT(3), YDOT(4),
  1      YDOT(5), YDOT(6)
15    FORMAT(7D20.8)
        END IF


    TOUT = TOUT + (TIME*3600)
     IF (ISTATE .LT. 0)  GO TO 80
40     CONTINUE
     STOP
80  WRITE(6,90)  ISTATE
90  FORMAT(///' Error halt.. ISTATE =',I3)
     STOP


   CONTINUE
 END PROGRAM MAIN
```

```
      SUBROUTINE DIFFUN(NEQ, T,Y,YDOT)


      IMPLICIT REAL*8 (A-H, O-Z)
      CHARACTER*8 METAL
      INTEGER  NEQ
        DOUBLE PRECISION  T, Y(6), YDOT(6), A(4), B(3), C(4), DUMMY, EDOT



      IF (TFINAL .NE. 0) GO TO 21
      OPEN (4, FILE='INPUT.txt', STATUS='OLD')
          IF (NEQ .EQ. 5) THEN
              READ (4, *) TFINAL, DUMMY, METAL, SIGMPA, TDEGC, G
          ELSE
              READ (4, *) TFINAL, EDOT, METAL, DUMMY, TDEGC, G
      END IF


      TFINAL = TFINAL * 3600


C***Define variables for Y(NEQ) 21  EPSILON=Y(1)
    RHOMAT=Y(2)
    RHOSTAT=Y(3)
    RHOBOUND=Y(4)
    RADIUS=Y(5)
    IF (NEQ .EQ. 6) THEN
    SIGAPP = Y(6)
    ELSE
    SIGAPP =SIGMPA/1.602D-19
```

```
      END IF


C***Define Constants & functions


      IF (METAL.EQ.'HT-9') THEN
        XJOG=0.0455
        Q=21.5
      ELSE
         XJOG=0.03
        Q=30
      END IF


!   GO TO 26 !23    XJOG=0.0455 !   Q=21.5


26  EGLIDE = 2.5
    ESELF = 2.8
    ZETA = 0.4


    DATA C1/2.055D-5/, C2/-1.015D-7/, C3/1.3D-10/
     1  D1/-1.9459D-2/, D2/57.241D0/
    DATA A(1)/1.178D1/, A(2)/-5.526D-4/, A(3)/-2.478D-6/,
     1  A(4)/6.89475D3/
      DATA B(1)/.254D0/, B(2)/1.54D-4/, B(3)/-1.26D-7/
    DATA C(1)/31.1D0/, C(2)/-1.359D-2/, C(3)/2.505D-5/, C(4)/-2.007D-8/
    DATA E1/213.28/, E2/-4.799D-2/, E3/-4.065D-6/
    DATA F1/2.0896/, F2/-4.218D-4/, F3/7.017D-7/, F4/-4.969D-10/
    DATA G1/0.2762/, G2/8.9309D-5/, G3/-6.262D-8/
```

```
PI                      =3.141592654
!XCRIT                  =2.D-7


IF (METAL.EQ.'HT-9') THEN
XCRIT                   =4D-6
ELSE IF (METAL.EQ.'F82H') THEN
XCRIT                   =1.5D-6
ELSE
XCRIT                   =2.D-7
END IF


HOLT                    =10.D0
DSO                     =2.D-1



BURG                    =2.58D-8
OMEGA                   =1.19D-23
!FREQ                   =1.D11



PRECRAD                 =C1+C2*TDEGC+C3*TDEGC**2


!IF (METAL.EQ.'HT-9') THEN
!PRECNUM                =DEXP(D1*TDEGC+D2)/1.0D10
!ELSE IF (METAL.EQ.'F82H') THEN
  PRECNUM               =DEXP(D1*TDEGC+D2)/1.0D10
```

```
!ELSE
!PRECNUM                    =DEXP(D1*TDEGC+D2)/1.0D6
!END IF


FPHASE                      =4.*PI*PRECRAD**3*PRECNUM/3.
SPACPRE                     =1./ SQRT(2*PRECNUM*PRECRAD)
TFAHR                       =TDEGC*9./5. +32.


  IF (METAL.EQ.'F82H') THEN


YOUNG                       =(233 - 0.0558*(TDEGC+273))*1.D9/1.D6
    POISSON                  =0.29
SMODLS                      =90.1 - 0.0209*(TDEGC+273)*1.D9/1.D6


ELSE IF (METAL.EQ.'HT-9') THEN


POISSON                     =G1+G2*TFAHR+G3*TFAHR*TFAHR
YOUNG                       =(E1+E2*TFAHR + E3*TFAHR*TFAHR)*1.D3
SMODLS                      =YOUNG/2./(1+POISSON)
ULTIMATE                    =(F1+F2*TFAHR+F3*TFAHR*TFAHR
 1                                 +F4*TFAHR*TFAHR*TFAHR)*6.944
ELSE
POISSON                     =B(1) + B(2)*TFAHR + B(3)*TFAHR*TFAHR
SMODLS                      =A(4)*(A(1)+A(2)*TFAHR+A(3)*TFAHR*TFAHR)
YOUNG                       =A(4)*(C(1) + C(2)*TFAHR + C(3)*TFAHR
1                                 *TFAHR+C(4)*TFAHR**3)
ULTIMATE                    =SMODLS*1.5D-2*(.6-2.47D-4*(TDEGC-400.))
```

91

```fortran
      END IF


!   GO TO 30 !25 POISSON
=G1+G2*TFAHR+G3*TFAHR*TFAHR !   YOUNG
=(E1+E2*TFAHR + E3*TFAHR*TFAHR)*1.D3 !   SMODLS
=YOUNG/2./(1+POISSON) !   ULTIMATE
=(F1+F2*TFAHR+F3*TFAHR*TFAHR
 !   1                              +F4*TFAHR*TFAHR*TFAHR)*6.944


30   CONTINUE

     ALFA                =1./PI/(1.-POISSON)
     SHEAR               =SMODLS/1.602D-19


     PPTN                =DLOG10(PRECNUM)
     PPTR                =PRECRAD*1.D8
     TEMP                =TDEGC+273.15
     BOLTZK              =1./8.617D-5/TEMP
     DGLIDE              =DSO*DEXP(-EGLIDE*BOLTZK)
     DSELF               =DSO*DEXP(-ESELF*BOLTZK)
     CMOBIL              =DSELF*BURG*BOLTZK
     TENSION             =SHEAR*BURG*BURG/3.5
     ARJOG               =XJOG*SHEAR*OMEGA
     CJOG                =DEXP(-ARJOG*BOLTZK)
```

```
RHOTOT=RHOMAT+RHOSTAT+RHOBOUND

SINKPPT=4.*PI*PRECNUM*PRECRAD

SINKTOT=SINKPPT+RHOTOT

GPRIME = .1*G/(3.15576D7)

DIF=2.*GPRIME/SINKTOT

IF (DSELF.LE.DIF) DSELF=DIF

HWALL=1./RHOSTAT/RADIUS

SPACDIS=1./ DSQRT(RHOMAT+RHOSTAT)

SPACING=1/(1/SPACDIS + 1/SPACPRE)

SIGMAT=SHEAR*BURG*DSQRT(RHOMAT)*ALFA

SIGWALL=SHEAR*BURG*DSQRT(RHOSTAT)*ALFA

SIGINTM=SHEAR*BURG*ALFA/SPACING


!SIGNOT = 100/1.602D-19

SIGEFF=SIGAPP-SIGINTM-SIGNOT


ARG=Q*OMEGA*SIGEFF*BOLTZK

Z1=DSELF/BURG

Z2=OMEGA*SIGMAT*BOLTZK

Z3=DLOG(1./ DSQRT(BURG*BURG*RHOMAT))

Z4=OMEGA*SIGWALL*BOLTZK

Z5=DLOG(1./ DSQRT (BURG/RADIUS))

VCMAT=CJOG*2.*PI*Z1*Z2/Z3

VCWALL=CJOG*2.*PI*Z1*Z4/Z5


IF (METAL.EQ.'HT-9') THEN

FREQ=1.5D12
```

```
      ELSE IF (METAL.EQ.'F82H') THEN
   FREQ=1D13
   ELSE
   FREQ=1D12
   END IF


   TEST=DSINH(ARG)
   VGLIDE=FREQ*SPACING*DSINH(ARG)*DGLIDE
   Y232=RHOMAT*DSQRT(RHOMAT)
   TRM21=VGLIDE*Y232
   TRM22=RHOMAT*VGLIDE/RADIUS
   TRM23=VCMAT*Y232
   TRM24=VGLIDE*XCRIT*RHOMAT*(RHOMAT+RHOSTAT)
   TRM33=VGLIDE*XCRIT*RHOMAT*RHOSTAT
   RTFRC=FPHASE*RADIUS/PI/PRECRAD
   IF (RTFRC.GE.1) RTFRC=1.
   RFACT=(1.- RTFRC)**2
   TRM32=2.*VCWALL*RHOSTAT/HWALL
   Z6=OMEGA*SHEAR*BOLTZK
   TRM51=3.*DSELF*Z6/(3.5*8.*RADIUS)


   YDOT(4)=(1.-2.*ZETA)*TRM32


   TRM52=RADIUS*YDOT(4)/RHOBOUND



C***Define YDOT(NEQ) except for YDOT(4), which has been defined
```

earlier

```
YDOT(1)=BURG*RHOMAT*VGLIDE

YDOT(2)=TRM21 -TRM22-TRM23-TRM24

YDOT(3)=TRM22-TRM32-TRM33

YDOT(5)=RFACT*TRM51-TRM52

YDOT(6)=(YOUNG*(EDOT - YDOT(1)))/1.602D-19



RETURN

END SUBROUTINE DIFFUN


SUBROUTINE JAC (NEQ, T, Y, ML, MU, PD, NROWPD)

  INTEGER  NEQ, ML, MU, NROWPD

  DOUBLE PRECISION  T, Y(*), PD(NROWPD,*)

END SUBROUTINE JAC


*DECK DLSODE

   SUBROUTINE DLSODE (F, NEQ, Y, T, TOUT, ITOL, RTOL, ATOL, ITASK,

  1                    ISTATE, IOPT, RWORK, LRW, IWORK, LIW, JAC, MF)
```

...DLSODE subroutine omitted due to length. Please refer to [48] for details.

APPENDIX B

Sample Input File

0.139   !Test Time(hrs)

0.0001   !Total Strain Rate(strain/s)

HT-9   !Material Type

150   !Stress(MPa), only used for creep analysis

232   !Operating Temperature(C)

0   !Irradiation amount

APPENDIX C

Sample Output File

```
TIME(HR)      P_STRAIN         RHOM             RHOS

0.1390D-02    0.10000000D-03   0.10000000D+11   0.10000000D+10

0.2780D-02    0.10000000D-03   0.10000000D+11   0.10000000D+10

0.4170D-02    0.10000000D-03   0.10000000D+11   0.10000000D+10

0.5560D-02    0.10000149D-03   0.10000003D+11   0.99999983D+09

0.6950D-02    0.10000322D-03   0.10000007D+11   0.99999963D+09

0.8340D-02    0.10000598D-03   0.10000013D+11   0.99999930D+09

0.9730D-02    0.10010155D-03   0.10000216D+11   0.99998819D+09

0.1112D-01    0.10170762D-03   0.10003640D+11   0.99980147D+09

0.1251D-01    0.14446820D-03   0.10094897D+11   0.99484738D+09

0.1390D-01    0.46177506D-03   0.10777485D+11   0.95909216D+09

0.1529D-01    0.93896097D-03   0.11819830D+11   0.90852684D+09

0.1668D-01    0.14261073D-02   0.12899650D+11   0.86062216D+09

0.1807D-01    0.19134017D-02   0.13991571D+11   0.81618937D+09

0.1946D-01    0.24006373D-02   0.15091373D+11   0.77499838D+09

0.2085D-01    0.28879001D-02   0.16195763D+11   0.73680488D+09

0.2224D-01    0.33752458D-02   0.17301781D+11   0.70139166D+09

0.2363D-01    0.38627313D-02   0.18406542D+11   0.66854443D+09

0.2502D-01    0.43503906D-02   0.19507561D+11   0.63807681D+09
```

```
0.2641D-01  0.48382558D-02  0.20602548D+11  0.60981489D+09

0.2780D-01  0.53263493D-02  0.21689562D+11  0.58360431D+09

0.2919D-01  0.58146934D-02  0.22766648D+11  0.55929020D+09

0.3058D-01  0.63033039D-02  0.23832000D+11  0.53672862D+09

0.3197D-01  0.67921976D-02  0.24884052D+11  0.51578346D+09

0.3336D-01  0.72813737D-02  0.25921632D+11  0.49634755D+09

0.3475D-01  0.77708212D-02  0.26943869D+11  0.47833291D+09

0.3614D-01  0.82605721D-02  0.27949353D+11  0.46160349D+09

0.3753D-01  0.87506107D-02  0.28937598D+11  0.44609099D+09

0.3892D-01  0.92409299D-02  0.29908093D+11  0.43172163D+09

0.4031D-01  0.97315470D-02  0.30859739D+11  0.41838877D+09

0.4170D-01  0.10222452D-01  0.31792319D+11  0.40603469D+09

0.4309D-01  0.10713640D-01  0.32705472D+11  0.39459222D+09
```

```
RHOB            RADIUS          STRESS          TOT_STRAIN


0.10000000D+10  0.10000000D-02  0.95517351D+02  0.50040000D-03

0.10000000D+10  0.10000000D-02  0.19103470D+03  0.10008000D-02

0.10000000D+10  0.10000000D-02  0.28655205D+03  0.15012000D-02

0.10000000D+10  0.10000000D-02  0.38206912D+03  0.20016000D-02

0.10000000D+10  0.10000000D-02  0.47758614D+03  0.25020000D-02

0.10000000D+10  0.10000000D-02  0.57310296D+03  0.30024000D-02

0.10000000D+10  0.10000001D-02  0.66860207D+03  0.35028000D-02

0.10000000D+10  0.10000001D-02  0.76381285D+03  0.40032000D-02

0.10000000D+10  0.10000001D-02  0.85116798D+03  0.45036000D-02

0.10000000D+10  0.10000001D-02  0.88611716D+03  0.50040000D-02

0.10000000D+10  0.10000001D-02  0.89054831D+03  0.55044000D-02
```

```
0.10000000D+10   0.10000001D-02   0.89307819D+03   0.60048000D-02
0.10000000D+10   0.10000001D-02   0.89557983D+03   0.65052000D-02
0.10000000D+10   0.10000001D-02   0.89809267D+03   0.70056000D-02
0.10000000D+10   0.10000001D-02   0.90060031D+03   0.75060000D-02
0.10000000D+10   0.10000001D-02   0.90309215D+03   0.80064000D-02
0.10000000D+10   0.10000001D-02   0.90555731D+03   0.85068000D-02
0.10000000D+10   0.10000001D-02   0.90798928D+03   0.90072000D-02
0.10000000D+10   0.10000001D-02   0.91038194D+03   0.95076000D-02
0.10000000D+10   0.10000001D-02   0.91273103D+03   0.10008000D-01
0.10000000D+10   0.10000001D-02   0.91503228D+03   0.10508400D-01
0.10000000D+10   0.10000001D-02   0.91728269D+03   0.11008800D-01
0.10000000D+10   0.10000001D-02   0.91947902D+03   0.11509200D-01
0.10000000D+10   0.10000001D-02   0.92162147D+03   0.12009600D-01
0.10000000D+10   0.10000001D-02   0.92371211D+03   0.12510000D-01
0.10000000D+10   0.10000001D-02   0.92574482D+03   0.13010400D-01
0.10000000D+10   0.10000001D-02   0.92772263D+03   0.13510800D-01
0.10000000D+10   0.10000001D-02   0.92964687D+03   0.14011200D-01
0.10000000D+10   0.10000001D-02   0.93151426D+03   0.14511600D-01
0.10000000D+10   0.10000001D-02   0.93332674D+03   0.15012000D-01
0.10000000D+10   0.10000001D-02   0.93508503D+03   0.15512400D-01
```

REFERENCES

[1] R. J. Amodeo and N. M. Ghoniem. Constitutive design equations for thermal creep deformation of ht-9, ppg-743. *University of California Report*, 1983.

[2] A. S. Argon and W. Moffatt. *Acta Metallurgica*, 29:293, 1981.

[3] M. F. Ashby. The influence of particles on boundary mobility. *Proc. 1st Riso Int. Symp. on Metallurgy and Materials Science Recrystallisation and Grain Growth of Multi-Phase and Particle Containing Materials.*, 1980.

[4] S. Mader H Rebstock A. Seeger, J. Diehl. Work-hardening and work-softening of face-centred cubic metal crystals. *Phil Mag*, 2:323, 1957.

[5] P. Haasen A. S. Argon. A new mechanism of work hardening in the late stages of large strain plastic flow in f.c.c and diamond cubic crystals. *Acta Metallurgica*, 41:3289–3306, 1993.

[6] Z. S. Basinski. Thermally activated glide in face-centred cubic metals and its application to the theory of strain hardening. *Phil Mag*, 4:393, 1959.

[7] Y. Bergstrom. A dislocation model for the stress-strain behavior of polycrystalline α-fe with special emphasis on the variation of the densities of mobile and immobile dislocations. *Materials Science and Engineering*, 5:193, 1970.

[8] R. Bullough and J. R. Willis. *Philosophical Magazine*, 31:855, 1975.

[9] K. D. Challenger and J. Moteff. *Metall Trans*, 4:749, 1973.

[10] A. H. Cottrell. *Prog. Metall. Physics*, 1:77, 1952.

[11] A. H. Cottrell. *Dislocations and Plastic Flow in Crystals*. Oxfored at the Clarendon Press, 1953.

[12] I. J. Cuddy. *Metall Trans*, 1:395, 1970.

[13] J. Moteff D. J. Michel and A. J. Lovell. *Acta Metallurgica*, 21:1269, 1973.

[14] U. Essmann and H. Mughrabi. Annihilation of dislocations during tensile and cyclic deformation and limits of dislocation densities.

[15] Y. Estrin and H. Mecking. A unified phenomenological description of work hardening and creep based on one-parameter models. *Acta Metallurgica*, 32:57–70, 1984.

[16] Y. Estrin. Dislocation theory based constitutive modelling: foundations and applications. *Materials Processing Technology*, 80-81:33–39, 1998.

[17] H. E. Evans and G. Knowles. *Acta Metallurgica*, 25:963, 1977.

[18] J. Friedel. *Dislocations*. Addison-Wesley Publishing Compan, Inc., 1964.

[19] A. S. Argon F. B. Prinz. The evolution of plastic resistance in large strain plastic flow of single phase subgrain forming metals. *Acta Metallurgica*, 32:1021–1028, 1984.

[20] D. Raabe F. Roters and G. Gottstein. Work hardening in heterogeneous alloys-a microstrutural approach based on three internal state variables. *Acta Materialia*, 48:4181–4189, 2000.

[21] N. M. Ghoniem and R. J. Amodeo. *Sol. State Phenom.*, 3 and 4:377, 1988.

[22] N. M. Ghoniem and K. Cho. The emerging role of multiscale modeling in nano- and micro-mechanics of materials. *J. Comp. Meth. Engr. Science*, 3(2):147–173, 2002.

[23] J. H. Gittus. Multiaxial mechanical equation of states for a work-hardening/recovery model of dislocation creep. *Philosophical Magazine*, 25:1233, 1972.

[24] J. H. Gittus. *Philosophical Magazine*, 35:293, 1977.

[25] J. H. Gittus. *Philosophical Magazine*, 39:829, 1979.

[26] J. Gittus. The mechanical equation of states: Disloction creep due to stresses varying in magnitude and direction. *Philosophical Magazine*, pages 1423–1440, 1971.

[27] A.S Argon G. Gottstein. Dislocation theory of steady state deformation and its approach in creep and dynamic tests. *Acta Metallurgica*, 35:1261–1271, 1987.

[28] P. T. Heald and M. V. Speight. *Philosophical Magazine*, 29:1075, 1974.

[29] D. Holt. *Journal of Applied Physics*, 41:3197, 1970.

[30] Hull. *Introduction to Dislocation*. Pergamon Press Ltd., 1969.

[31] U.F. Kocks H. Mecking. Kinetics of flow and strain-hardening. *Acta Metallurgica*, 29:1865–1875, 1981.

[32] ANSYS Inc. Ansys 7.1 documentation. 2003.

[33] T.J.R Hughes J.C. Simo. *Computational Inelasticity.* Springer, 1998.

[34] W. G. Johnson and J. J. Gilman. *Journal of Applied Physics*, 30:129, 1950.

[35] R. D. Martinez Jr. The influence of crystal surfaces on dislocation behavior in mesoscopic plasticity: A combined dislocation dynamics-finite element approach. Master's thesis, University of California, Los Angeles, 2000.

[36] J. Lothe J. P. Hirth. *Theory of Dislocations.* John Wiley and Sons, Inc., 1982.

[37] K.Domkin. A brief review of physically based material models. 2001.

[38] U. F. Kocks. A statistical theory of flow stress and work-hardening. *Phil Mag*, 13:541, 1966.

[39] T. G. Langdon. Dislocations and creep. *Proc. Conf. on Dislocations and the Properties of Real Materials, Royal Society of London*, page 221, 1984.

[40] J. C. M. Li. *Journal of Applied Physics*, 33(10), 1962.

[41] A. Mendelson. *PLASTICITY: theory and application.* Robert E. Krieger Publishing Company, Inc., 1968.

[42] H. Mughrabi. A two-parameter description of heterogeneous dislocation distributions in deformed metal crystals. *Materials Science and Engineering*, 85:15–31, 1987.

[43] H. Mughrabi. Dislocation clustering and long-range internal stresses in monotonically and cyclically deformed metal crystals. *Revue Phys Appl*, 23:367–379, 1988.

[44] W. Blum M. Meier. Modelling high temperature creep of academic and industrial meterials using the composite model. *Materials Science and Engineering*, A164:290–294, 1993.

[45] F. R. N. Nabarro. Steady-state diffusional creep. *Philosophical Magazine*, page 231, 1967.

[46] N. Kioussis N. M. Ghoniem, E. P. Busso and H. Huang. Multiscale modelling of nanomechanics and micromechanics: an overview. Philosophical Magazine, received 4 June 2003, 2003.

[47] R. J. Amodeo N. M. Ghoniem, J. R. Matthews. A dislocation model for creep in engineering materials. *Res Mechanica*, 29:197–219, 1990.

[48] K. Radhakrishnan and A. C. Hindmarsh. Description and use of lsode, the livermore solver for ordinary differential equations. *LLNL report UCRL-ID-113855*, 1993.

[49] H. Rauh and R. Bullough. *Philosophical Magazine*, 52:33, 1985.

[50] M. W. Finnis R. Bullough and M. H. Wood. *Journal of Nuclear Materials*, 103:1263, 1981.

[51] B. H. Forsen R. Lagneborg and J. Wiberg. A recovery-creep model based upon dislocation distributions. *The Materials Society, London*, pages 1–7, 1974.

[52] W. Blum R. Sedláček. Microstructure-based constitutve law of plastic deformation. *Computational Materials Science*, 25:200–206, 2002.

[53] Rolf Sandstrom. On recovery of dislocations in subgrains and subgrain coalescence. *Acta Metallurgica*, 25:897–904, 1977.

[54] Rolf Sandstrom. Subgrain growth occuring by boundary migration. *Acta Metallurgica*, 25:905–911, 1977.

[55] J. P. Robertson S. J. Zinkle and R. J. Klueh. Thermophysical and mechanical properties of fe-(8-9)activation steel. *Oakridge National Lab*, 1998.

[56] A. S. Argon S. Takeuchi. Steady-state creep of single-phase crystalline matter at high temperature. *Journal of Applied Materials Science*, 11:1542–1566, 1976.

[57] A. S. Argon S. Takeuchi. Stead-state creep of alloys due to viscous motion of dislocations. *Acta Metallurgica*, 24:883, 1976.

[58] W.L. Bell T. Lauritzen and S. Vaidyanathan. Effects of irradiation on the mechanical properties of ferritic alloys ht-9 and 2.25r-1mo. *Proceedings of Topical Conference on Ferritic Alloys for use in Nuclear Energy Technologies*, pages 623–630, 1983.

[59] E. Voce. *Inst Metals*, 74:537, 1948.

[60] G. A. Webster. *Philosophical Magazine*, 14:775, 1966.

[61] Yngve Bergstrom William Roberts. The stress-strain behavior of single crystal and polycrystal of face-centered cubic metals-a new dislocation treatment. *Acta Metallurgica*, 21:457–469, 1973.

[62] A. Cegielska W. Blum, A. Rosen and J. L. Martin. Two mechanisms of dislocation motion during creep. *Acta Metallurgica*, 37:2439–2453, 1989.

[63] S. Vogler W. Blum and M. Biberger. Stress dependence of the creep rate at constant dislocation structure. *Materials Science and Engineering*, A112:93–106, 1989.

[64] Jr. W. T. Read. *Dislocations in Crystals*. McGraw-Hill Book Company, Inc., 1953.

[65] H. Hallén Y. Bergstrom. An improved dislocation model for the stress-strain behavior of polycrystalline α-fe. *Materials Science and Engineering*, 55:49–61, 1982.

[66] Y. Brechet Y. Estrin, H. Braasch. A dislocation density based constitutive model for cyclic deformation. *Journal of Engineering Materials and Technology*, 118:441, 1996.

[67] M.t L. Hamilton T. Hirose Y. Katoh Y. Kohno, A. Kohyama and F. A. Garner. Specimen size effects on the tensile properties of jpca and jfms. *Journal of Nuclear Materials*, 283-287.

[68] M. Zehetbauer. Cold work hardening in stages iv and v of f.c.c metals-ii. model fits and physical results. *Acta Metallurgica*, 41:589–599, 1993.